UNIVERSIDADE FEDERAL DE SANTA CATARINA
CAMPUS TECNOLOGICO
AUTOMATION AND SYSTEMS ENGINEERING GRADUATE PROGRAM

Paulo Henrique Foganholo Biazetto

Development of an optimal control strategy for temperature regulation and thermal storage operation of a solar power plant

Florianópolis - SC
2021

Paulo Henrique Foganholo Biazetto

Development of an optimal control strategy for temperature regulation and thermal storage operation of a solar power plant

Dissertation presented to the Automation and Systems Engineering Graduate Program of the Universidade Federal de Santa Catarina in partial fulfillment of the requirements for the degree of Master in Automation and Systems Engineering.
Supervisor: Prof. Gustavo Artur de Andrade, Dr.

Florianópolis - SC
2021

Ficha de identificação da obra elaborada pelo autor,
através do Programa de Geração Automática da Biblioteca Universitária da UFSC.

Biazetto, Paulo Henrique
Development of an optimal control strategy for temperature regulation and thermal storage operation of a solar power plant / Paulo Henrique Biazetto ; orientador, Gustavo Artur de Andrade, 2021.
80 p.

Dissertação (mestrado) - Universidade Federal de Santa Catarina, Centro Tecnológico, Programa de Pós-Graduação em Engenharia de Automação e Sistemas, Florianópolis, 2021.

Inclui referências.

1. Engenharia de Automação e Sistemas. 2. Produção de energia. 3. Controle ótimo. 4. Energia renovável. 5. Energia solar térmica. I. de Andrade, Gustavo Artur. II. Universidade Federal de Santa Catarina. Programa de Pós Graduação em Engenharia de Automação e Sistemas. III. Título.

Paulo Henrique Foganholo Biazetto

Development of an optimal control strategy for temperature regulation and thermal storage operation of a solar power plant

The present work in the Master level was evaluated and approved by the examining board composed of the following members:

Prof. Eduardo Camponogara, Dr.
Universidade Federal de Santa Catarina

Prof. Marcelo De Lellis Costa de Oliveira, Dr.
Universidade Federal de Santa Catarina

Prof. Marcus Vinícius Americano, Dr.
Universidade Federal da Bahía

This Dissertation is recommended in partial fulfillment of the requirements for the degree of “Master in Automation and Systems Engineering”, which has been approved in its present form by the Automation and Systems Engineering Graduate Program Master in Automation and Systems Engineering.

Documento assinado digitalmente
Werner Kraus Junior
Data: 20/08/2021 17:51:37-0300
CPF: 531.085.239-53
Verifique as assinaturas em https://v.ufsc.br

Graduate Program Coordinator

Documento assinado digitalmente
Gustavo Artur de Andrade
Data: 20/08/2021 15:56:14-0300
CPF: 066.316.109-66
Verifique as assinaturas em https://v.ufsc.br

Prof. Gustavo Artur de Andrade, Dr.
Supervisor

Florianópolis - SC, 2021.

This work is dedicated to my professors, my dear parents and friends.

ACKNOWLEDGEMENTS

This work was partially supported by CNPq and Petrobras.

RESUMO

Nesta dissertação de mestrado, uma Estratégia de Controle Ótimo para plantas solares térmicas é proposta. Para isso, inicialmente, um modelo matemático fenomenológico do campo de coletores solares e do sistema de armazenamento de energia térmica são estudados e desenvolvidos levando em consideração as principais características da planta. Os tanques têm importância fundamental em plantas solares, pois permitem o desacoplamento entre os sistemas de captação de energia solar e de armazenamento de energia térmica. Graças a esta propriedade, os objetivos de controle podem ser desacoplados e o sistema de controle proposto é projetado de forma descentralizada: um controlador ótimo que visa obter a trajetória ótima dos estados do campo de coletores solares, minimizando uma função de custo associada ao rastreamento de referência da temperatura; e outra para calcular a política de controle ótima para o armazenamento/despacho dos tanques térmicos, de acordo com perfis tarifários de energia variáveis. A metodologia é considerada com uma perspectiva rigorosa para mostrar o que pode ser efetivamente garantido com ela. Além disso, é discutida sua implementação prática por meio de uma abordagem direta, na qual o controlador é transformado em um problema de programação não linear. Vários resultados de simulação com tarifas de energia e dados meteorológicos do Brasil e da Espanha são apresentados para ilustrar o desempenho da metodologia proposta. Por fim, um estudo comparativo com duas estratégias clássicas de controle mostra as melhorias na receita de energia produzida nesses cenários. São estimados ganhos de até 13.6% em termos de receita anual, caso a Estratégia de Controle Ótimo seja adotada.

Palavras-chave: Produção de energia; Controle ótimo; Energia renovável; Energia solar térmica.

RESUMO EXPANDIDO

Introdução

O consumo global de energia e eletricidade está aumentando rapidamente devido ao crescimento da população, industrialização e urbanização. Como as fontes de combustível fósseis estão se esgotando e emitem gases do efeito estufa, o mundo está investindo em tecnologias de geração de energias renováveis, limpas e eficientes. Pesquisas têm mostrado que as fontes de energia solar, eólica e biomassa são as mais promissoras e podem contribuir para o aumento da produção energética e redução dos impactos ambientais ocasionados pela queima dos combustíveis fósseis. Dentre as fontes de energia renovável, o Brasil tem um grande potencial para o aproveitamento de energia solar térmica devido à sua localização geográfica e características climáticas.

Sistemas de geração de energia solar térmica são compostos por um campo de coletores solares, um ciclo de potência e um sistema de armazenamento térmico que permite que a planta opere com horários escalonados. Assim, os objetivos de controle destes sistemas são maximizar a energia solar captada no campo de coletores solares e a receita de energia elétrica no bloco de potência de acordo com uma tarifa de energia. Os sistemas de controle são complexos devido às características não lineares e multivariáveis, bem como às várias restrições de operação da planta. Se comparado com os países detentores da tecnologia, o Brasil ainda possui carência de conhecimentos para projeto e operação de tais sistemas. Neste sentido, técnicas de controle avançado e otimização terão que ser desenvolvidas levando em consideração as características particulares do clima e sistema de tarifas da venda de eletricidade no Brasil, o que gera um conhecimento específico para o desenvolvimento de tecnologia local.

Nesta dissertação, uma estratégia de controle ótimo para plantas solares térmicas é proposta. Para isso, um modelo matemático fenomenológico é primeiramente estudado e desenvolvido levando em consideração as principais características da planta. Graças às propriedades físicas dos subsistemas envolvidos, os objetivos de controle podem ser desacoplados e o sistema de controle proposto é projetado de forma descentralizada: um controlador ótimo que visa obter a trajetória ótima dos estados do campo de coletores solares, minimizando uma função custo associada ao rastreamento de referência de temperatura; e outro para calcular a política de controle ótimo para o armazenamento/despacho dos tanques de armazenamento térmico. A metodologia é considerada com uma perspectiva rigorosa de forma a mostrar o que pode ser efetivamente garantido com a utilização dela. Além disso, sua implementação prática é discutida através de uma abordagem direta, na qual o controlador é transformado para um problema de programação não linear. Diversas simulações com tarifas de energia e dados meteorológicos do Brasil e Espanha são apresentados para ilustrar o desempenho da metodologia proposta. Por fim, um estudo comparativo com duas estratégias de controle clássicas apresenta as melhorias na receita da energia produzida nestes cenários de simulação. São estimados ganhos de até 13.6% em termos de receita anual, caso a estratégia de controle ótimo seja adotada.

Objetivos

Objetivo geral

O objetivo geral desta dissertação de mestrado é contribuir para o desenvolvimento de sistemas de controle de plantas solares térmicas maximizando a energia solar capturada e o despacho do sistema de armazenamento de energia térmica para o bloco de potência. Para isto, é proposto o uso da teoria de controle ótimo para projeto de tal controlador.

Objetivos específicos

Para alcançar o objetivo geral, são definidos os objetivos específicos a seguir:

- Revisão do estado da arte das usinas de energia solar térmica com base na tecnologia de coletor Fresnel linear;
- Modelar matematicamente o campo de coletores solares e tanques de armazenamento de energia térmica;
- Formulação do problema de controle e a sua função custo a ser otimizada;
- Simular e analisar os resultados obtidos de acordo com o comportamento esperado;
- Comparar os resultados obtidos com estratégias clássicas de controle.

Metodologia

O projeto consiste em uma revisão bibliográfica de técnicas de controle ótimo aplicado em planta solares térmicas, modelagem do sistemas de captação de energia e de armazenamento térmico, implementação do controlador ótimo com as restrições operacionais da planta e simulação dos processos de controle desenvolvidos.

Cada subsistemas da planta é modelado baseado em resultados estabelecido na literatura. Os modos de operação são definidos de acordo com as características operacionais da planta considerada neste trabalho. Os tanques apresentam importância fundamental em plantas solares, pois permitem o desacoplamento entre o sistema de captação da energia solar e o sistema de armazenamento de energia térmica. Graças a essa propriedade, são estudados a formulação de dois controladores ótimos desenvolvidos de forma descentralizada, responsáveis pela otimização da captação de energia solar e do armazenamento/despacho da energia térmica do tanque quenta para o bloco de potência de acordo com perfis de tarifa energética variáveis. Sendo assim, com dados reais de perturbações e de tarifas energéticas, o processo é simulado com os controladores implementados e uma análise da resposta do sistema é realizada.

Resultados e Discussão

Dois cenários são executados para a validação do processo e do controlador desenvolvido. Primeiramente, uma simulação do sistema com dados meteorológicos do Brasil e suas respectivas tarifas energéticas é realizada avaliando a capacidade do sistema de controle em manter a planta dentro ponto de operação projetado. Na sequência, dados meteorológicos e normas de tarifas energéticas da Espanha são considerados nas simulações visando corroborar com os resultados obtidos.

Por fim, duas estrategias clássicas de controle são implementadas para realizar um es-

tudo comparativo com controlador ótimo proposto. Em particular, é analisado a receita de energia, propriedades de seguimento de referência da temperatura de saída no campo solar e temperatura do tanque frio, desfoque dos espelhos, modos de operação e restrições operacionais.

Considerações Finais
O controlador ótimo proposto apresentou resultados melhores que as estratégias clássicas. Para o cenário Brasileiro, foram obtidos ganhos na receita anual de até 13.6%, enquanto que ganhos de 5.4% foram observados para um período de seis dias no contexto Espanhol. É importante enfatizar que estes resultados consideram apenas uma configuração de planta solar e os resultados podem variar de acordo com a capacidade de armazenamento da planta e tamanho do campo solar. Além disso, as simulações consideraram um cenário ideal do problema de controle, isto é, conhecimento da radiação solar futura e combinação perfeita entre o modelo e a dinâmica da planta. Dessa forma, o desempenho alcançado representa um limite teórico de operação do sistema, sendo que na prática o sistema de controle terá que enfrentar erros de modelagem, perturbações não modelados e previsões de tempo incertas.

Palavras-chave: Produção de energia; Controle ótimo; Energia renovável; Energia solar térmica.

ABSTRACT

In this master's dissertation, an Optimal Control Strategy for thermal solar power plants is proposed. For this, first, a phenomenological mathematical model of the solar collector field and thermal energy storage systems are studied and developed, taking into account the main characteristics of the plant. The tanks have fundamental importance in solar plants, allowing the decoupling between the solar energy capture and the thermal energy storage systems. Thanks to this property, the control objectives can be decoupled and the proposed control system is designed in a decentralized manner: an optimal controller that aims to obtain the optimal trajectory of the states of the solar collector field, minimizing a cost function associated with the temperature reference tracking; and another to calculate the optimal control policy for the storage/dispatch of the thermal tanks, according to variable energy tariff profiles. The methodology is considered with a rigorous perspective to show what can be effectively guaranteed using it. In addition, its practical implementation through a direct approach, in which the controller is transformed into a non-linear programming problem, is discussed. Several simulation results with energy tariffs and meteorological data from Brazil and Spain are presented to illustrate the performance of the proposed methodology. Finally, a comparative study with two classic control strategies shows the improvements in the energy revenue produced in these scenarios. Gains of up to 13.6% are estimated in terms of annual revenue if the Optimal Control Strategy is adopted.

Keywords: Energy production; Optimal control; Renewable energy; Thermal solar power plants.

LIST OF FIGURES

LIST OF TABLES

LIST OF ABBREVIATIONS AND ACRONYMS

AD	Algorithmic Differentiation
BVP	Boundary Value Problem
CAS	Computer-algebra System
CSP	Concentrating Solar Power
HTF	Heat Transfer Fluid
IAM	Incident Angle Modifier
LCOE	Levelized Cost of Energy
MIBEL	Mercado Ibérico de Eletricidade
NLP	Nonlinear programming
OCP	Optimal Control Problem
ODE	Ordinary Differential Equation
OMIE	Iberian Energy Market Operator
PMP	Pontryagin's maximum principle
PPA	Power Purchase Agreement
SPA	Solar Position Algorithm
TES	Thermal Energy Storage
TOD	Time Of the Day

LIST OF SYMBOLS

T	Temperature
h	Specific enthalpy
ρ	Specific mass
c_p	Specific heat
m	Mass flow rate
α	Efficiency
γ	Defocus
L	Liquid Level
S	Length
G	Aperture
I	Radiation
A	Area
H	Enthalpy
Q	Power provided by electrical resistance
P_w	Price of the electricity produced
TOD	Time of day
PPA	Power Purchase Agreement
η	Number of loops
β	Boolean function
c	Constant
θ	Angle (degrees)
σ	Angle (radians)
IAM	Incident angle modifier
SW	Solar-weighted mirror reflectivity
DM	Dirt on mirror derate
EM	General optical error derate
$\tilde{H}_l$	Thermal losses by convection in the solar field
$\tilde{P}_l$	Thermal losses by convection in the TES
$\mathcal{H}$	Hamiltonian
$\mathcal{L}$	Lagrangian
λ	Costate
μ	Lagrangian multipliers
J	Cost function

SUBSCRIPTS AND SUPERSCRIPTS

tf	Cold TES system
tq	Hot TES system
amb	Ambient
m	Average
c	Solar collector field
p	Power block
a	Absolute continuous
d	Step function
op	Optical
e	Pipe
tr	Transversal
lo	Longitudinal
de	Topocentric sun declination
hr	Topocentric local hour
gl	Geocentric latitude
ze	Topocentric zenith
az	Topocentric azimuth
ref	Reference
rec	Value to switch between the start-up and nominal operating modes
min	Minimum
max	Maximum
mop	Minimum operating
opt	Optimal value

CONTENTS

1 INTRODUCTION

1.1 MOTIVATION

Sustainability with the environment and low pollutant emissions are the main driving forces behind efforts to utilize various sources of renewable energy. The use of renewable energies was greatly boosted during the 1970s, due to the first major oil crisis. With the consequent economic instability in the oil sector, interest in ways of generating alternative energy has emerged (CAMACHO, E. et al., 2012). In addition to the economic concern, the environmental factor gained prominence due to the increase mainly in carbon dioxide emissions. The use of renewable energies seeks to reduce the environmental impacts caused by fossil fuels. These are being consumed at an accelerated pace, at the same time as the energy demand is increasing on the planet.

In the last four decades, the world energy demand and carbon dioxide (CO_2) production have more than doubled and, according to the projections in Agency (2020a) which incorporates existing energy policies as well as an assessment of the results likely to stem from the implementation of announced political intentions, an increase of 6.19% in the world production of CO_2 is expected until 2040. In a scenario of sustainable development with public policies that outlines an integrated approach to achieving internationally agreed objectives on climate change, air quality and universal access to energy, it is expected that CO_2 emissions would reduce 52.86%. The CO2 emissions data by region and perspective for global emissions in the 2040 scenario are shown in Figure 1.

In 2018, only 9.8% of the total energy generated in the world came from renewable sources, considering hydro, this value reaches up to 25.6% (AGENCY, 2020b). In the same period, Brazil is the third country in the world in the production of renewable energies with 495 TWh, behind only China and the United States. However, despite the good results, in the last ten years, Brazil has been experiencing a significant increase in the use of non-renewable energy sources, as can be seen in Figure 2.

According to the 2020 National Energy Balance Report with the base year 2019 (MINAS E ENERGIA, 2020a), of the total electricity generated in the country in that year, 64.9% came from hydraulic energy, while 14.6% came from oil products, coal, and natural gas. Nuclear energy accounted for 2.5% of the total electricity produced and biomass 8.4%. Other renewable and non-renewable sources produced 9.6% of the country's total electricity that year.

In Brazil, investment in solar energy has increased a lot in recent years and several regions of the country have favorable conditions to exploit this energy source (TIBA, 2000). According to the Ten-Year Energy Expansion Plan (MINAS E ENERGIA, 2020b), the share of solar energy in total electricity produced in 2030 will be more than 4%. In addition, the perspective for the coming years is that renewable energy

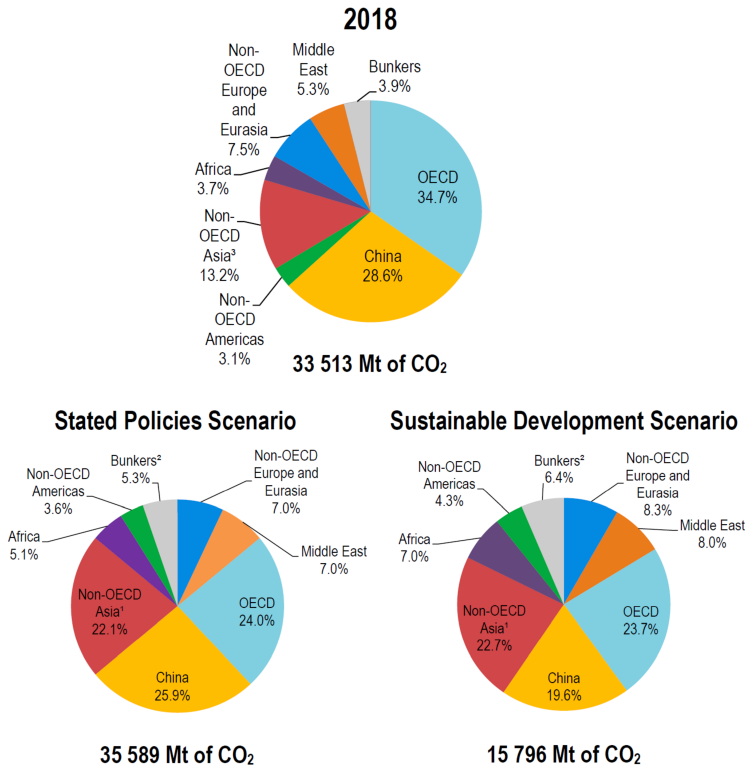

Figure 1 – CO2 emissions data by region and perspectives for global CO2 emissions by region in the 2040 scenario. Adapted from Agency (2020a).

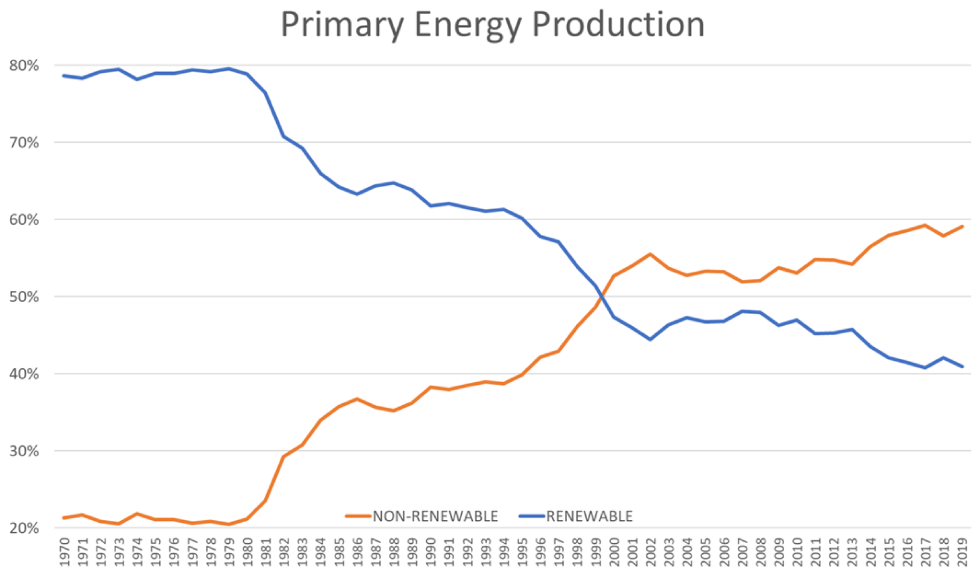

Figure 2 – Primary Energy Production. Adapted from Minas e Energia (2020a).

sources will increase their total contribution, representing 86% of the installed electricity generation capacity.

1.2 THE SUN AS RENEWABLE ENERGY

Among the available renewable energy sources, solar radiation is one of the most promising. Each year, the sun supplies 150000 TW of power to Earth, where about half of this energy reaches the Earth's surface while the other half is reflected to outer space by the atmosphere. This amount represents approximately 10000 times the energy that humanity currently needs (CAMACHO, E. et al., 2012). Moreover, it is estimated that the radiation from the sun can be supplied for more than 5 billion years. Based on these studies, several technologies have emerged in order to harvest, store, convert and utilize solar energy.

1.2.1 Concentrating solar power plants

Currently, there are two main technologies that harvest solar energy: (i) Concentrating Solar Power (CSP); and (ii) solar photovoltaic. A CSP plant is represented as a complex network, where each component has stationary and start-up losses, in which it needs attention and maintenance. However, a considerable advantage of these systems, compared to the photovoltaic option, is that they can integrate Thermal Energy Storage (TES) systems, allowing to reduce the mismatch between supply and demand through suitably managing the time periods of energy charge and discharge. A comprehensive review of CSP plants and some new concepts for the integration of TES systems into them can be found in Pelay et al. (2017) and Alva et al. (2018).

A schematic diagram of a CSP plant based on Fresnel reflectors is presented in Figure 3. Basically, the plant consists of a solar collector field, thermal storage tanks, and a power cycle. The main purpose of the solar collector field is to increase the temperature of the Heat Transfer Fluid (HTF) to provide the desired outlet temperature in an operating range. The fluid is then sent toward the TES system. The energy stored in the hot TES is discharged to produce electricity whenever needed. Note that the storage unit completely decouples the power block from the solar field allowing to control the power delivered to the conversion cycle to better meet variable-price tariffs (GONZÁLEZ-PORTILLO et al., 2017).

From a control point of view, the control strategies for CSP systems aim at maintaining the solar collector outlet temperature close to its nominal value in spite of disturbances by varying the HTF mass flow rate. In this context, many methodologies have been proposed in the literature. The approaches range from linear feedback controllers (CIRRE et al., 2007; BARAO et al., 2002) to model-based predictive controllers (CAMACHO, E. et al., 2012, 2007b; LEMOS et al., 2014; ANDRADE et al., 2013) or

(a) Facilities and laboratories available at the Plataforma Solar de Almería.

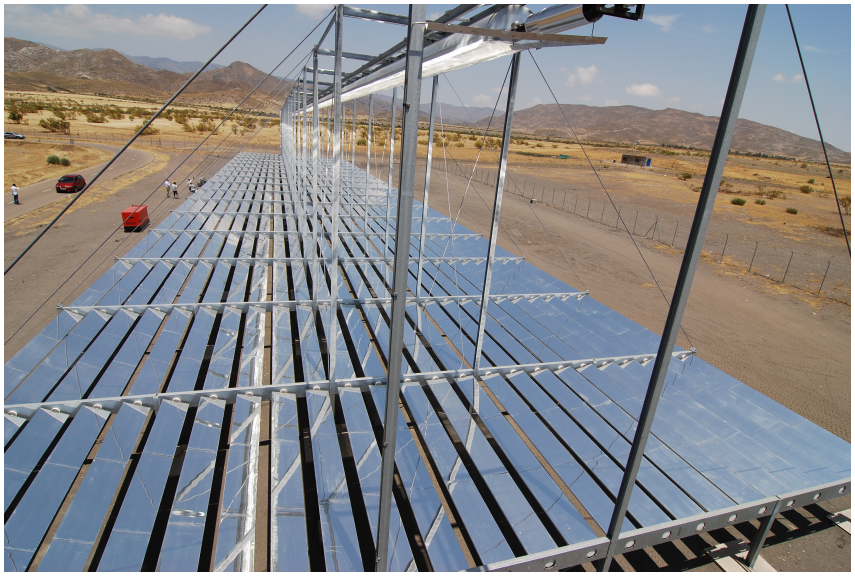

(b) Linear Fresnel concentrator FRESDEMO at the Plataforma Solar de Armería.

Figure 3 – Almería Solar Platform. Images obtained from Almería (2021)

adaptive control (LEMOS et al., 2014). A survey containing the main control strategies applied in CSP since the 1980s can be seen in E. F. Camacho et al. (2007a,b).

When a TES system is integrated into the CSP plant, an additional control variable – the mass flow rate from the storage tank to the power block – can be included in the control problem in order to exploit the dispatchability capacities of the overall system. In this case, the Levelized Cost of Energy (LCOE) decreases even more. Recent works, such as Sioshansi and Denholm (2010), Wittmann et al. (2011), Madaeni et al. (2011), Casati et al. (2015), Javad Mahmoudimehr and Loghmani (2016) and J. Mahmoudimehr and Sebghati (2019), developed methodologies based on optimization techniques for the performance management of CSP plants equipped with TES systems.

In this work, an optimal control methodology is proposed to maximize the usage of the thermal energy captured by CSP plants in order to generate electricity in a

variable-price tariff scenario. This framework is currently adopted in countries such as USA, Spain and Brazil, among several others. Our approach considers two decentralized optimal controllers: one for the reference tracking of the solar collector field outlet temperature; and another one for the dispatch of the thermal energy to the power block. One important factor considered in the cost function of the optimal dispatch controller is the Power Purchase Agreement (PPA), which is a previously negotiated agreement for the purchase and sale of long-term clean energy for a specific asset and at a pre-fixed price, multiplied by the Time Of the Day (TOD), a pre-set tariff factor corresponding to the power value produced at peak times. Both factors are considered in order to balance investment and operating costs to make a profit. The control design is considered with a rigorous perspective and the main industrially relevant constraints are imposed into the problem in order to show what can effectively be guaranteed with our approach on the long run. A quantitative study on the performance of the proposed methodology compared to a classic strategy widely used in practice is presented considering different numerical scenarios together with performance indexes.

This dissertation was developed in the context of the research project “Enhancement and Validation of Simulation Platform of Linear Concentration Heliotothermic Plants with Technological Innovation Studies” (in Portuguese) agreed between Petrobras and Universidade Federal de Santa Catarina, where the supervisor of this dissertation was a research team member. For this reason, some of the numerical values of the plant parameters were not described or made adimensional for sake of secrecy. However, the results developed in this document are presented, whenever possible, in a general framework in order to reach a relevant portion of the scientific community.

1.3 OBJECTIVES

1.3.1 General Objective

The general objective of this master thesis is to contribute with the development of control systems for the maximization of capture of solar radiation by the solar field and the dispatch of the hot thermal energy storage system to the power block. It is proposed the use of the optimal control theory of such controller.

1.3.2 Specific Objectives

The specific objectives for performing the study defined in the general objectives are presented below:

- Review of the state of the art of thermal solar power plants based on linear Fresnel collector technology;

- Mathematical modeling of the solar collector fields and thermal energy storage tanks;
- Formulation of the control problems and the cost functions to be optimized;
- Analyze the results of the simulation according to the expected behavior;
- Compare the results obtained with classical control strategies.

1.4 ORGANIZATION OF THE DISSERTATION

This dissertation is organized as follows:

Chapter 2 describes the solar power plant under consideration in this work and the mathematical modelling of the most important subsystems involved in the thermal solar process, including the operation modes. The plant is based on indirect steam generation technology, where a heat transfer fluid is used to absorb the heat from the solar irradiation and to transfer it to the water in order to generate steam. The modelling of each subsystem was based on established results of the literature and brought together to simulate the plant. In this chapter, the control problem is also described in detail. In particular, the control system must track the outlet temperature of the solar collector field and dispatch the thermal energy to the power block according to a variable-price tariff scenario.

The proposed Optimal Control Strategy is described in Chapter 3. First, the theoretical background of optimal control theory is introduced focusing on indirect and direct implementation methods. Then, the optimal control system of solar power plant is formulated. Thanks to the physical properties of the subsystems involved in the plant, the control objectives can be decoupled and the control system is designed in a decentralized manner: an optimal controller that aims to obtain the optimal trajectory of the solar collector field states by minimizing a cost function associated with the temperature reference tracking; and another one to compute the optimal control policy for the storage/dispatch of the thermal tanks. The methodology is considered with a rigorous perspective in order to show what can effectively be guaranteed by using such decentralized approach.

The numerical results of the proposed control strategy are presented and discussed in Chapter 5. Extensive simulations with realistic energy tariff prices and weather data of Brazil and Spain are presented. Furthermore, a comparative study with two classic control strategies illustrate the improvements in the revenue of the produced energy in such scenario. For the particular case of the Brazilian scenario, 365 days were considered and potential gains up to 13.63% in terms of yearly revenue are estimated, in case the optimal strategy is adopted.

Finally, the concluding remarks and future works are discussed in Chapter 6.

2 SYSTEM MODELING

This chapter presents the solar power plant studied in this dissertation. More precisely, it is described the main equipment and processes involved in the capture of solar energy and its conversion into thermal energy, and the storage/dispatch of this energy to the power block in order to generate electricity. The different operating modes of the plant are also studied since they are very important for the proper operation and control of the system. Then, the mathematical modelling of the main subsystems is proposed. This result is based on very well-established results from literature and brought together to describe the behavior of the whole process. Finally, the control problem, together with the controlled and manipulated variables, and the main disturbances is presented.

2.1 PLANT DESCRIPTION

The CSP system proposed in this work to test the Optimal Control Strategy is depicted in Figure 4. As it was already presented in Chapter 1, this system is composed of a solar collector field based on the Fresnel technology, thermal storage tanks, and a power cycle. The solar collectors are distributed and organized in lines forming a structure of parallel loops. They are interconnected by a feed centrifugal pump that pumps the HTF from the cold TES system to the entire solar field.

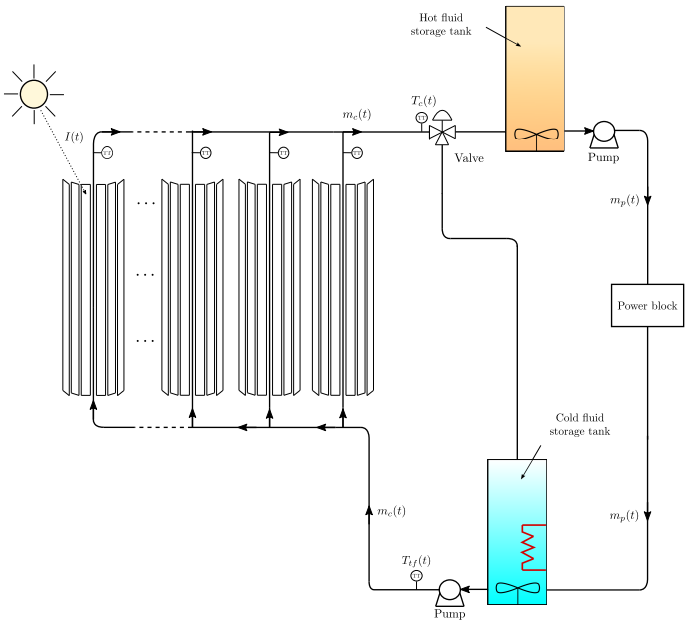

Figure 4 – Schematic diagram of the solar plant considered in this work.

The solar collector field is the main source of energy for the system to raise the temperature of the HTF in order to cover the heat demand of the power block. In the case of the Fresnel collectors, the conversion of radiant energy into thermal energy

occurs through the reflection of the sunlight by the mirrors in the heat pipe absorber, in which the HTF circulates. In this work, the HTF will be an anhydrous ternary mixture, composed of $Ca(NO3)2$, $KNO3$, $NaNO3$, generically called molten salts. The main characteristics of this mixture are the high heat transfer coefficient, thermal stability, low cost and not being flammable.

The tanks aim to store the energy of the HTF and decouple the collector field from the power block. The hot TES system stores the fluid coming from the solar field, while the cold TES system stores the fluid during the plant *start-up* process, after the power generation, and night and *anti-freeze* operation. As can be seen in Figure 4, both TES systems are positioned in series with the solar collector field, however, a valve is used to change the plant's operating modes.

2.1.1 Operation Modes

The solar power plant considered in this work has several constraints that must be taken into account during its operation. These constraints can be translated into the following operating modes (see Figure 5), which are defined by switching the valve located at the end of the solar field based on the values of the incident radiation and the HTF temperature:

- **Start-up:** The HTF recirculates between the cold TES system and the solar collector field through the centrifugal pump. This operating mode only happens during the light phase of the day and lasts until the outlet temperature of the solar collector field reaches a minimum outlet temperature value, $T_{c,rec}$.
- **Nominal:** During nominal operation, the outlet temperature of the solar collector field is set to its nominal reference temperature, $T_{c,ref}$. The HTF moves from the solar field to the hot TES, which will then feed a heat exchanger in the power block in order to generate steam for a turbine. After being used in the heat exchanger, the HTF returns to the cold TES and is pumped to the solar collector field to restart the cycle again.
- **Shut-down:** During this mode, the hot TES system stops receiving fluid from the solar field. The field starts to work recirculating the fluid in the cold TES system. The hot fluid dispatch continues until all the fluid from the hot tank runs out.
- **Night and anti-freeze:** This operation mode aims to keep the temperature limits within an acceptable and safe range, mainly conditioning the fluidity of the HTF in the pipelines. An electrical resistance inside the cold TES system is used to induce heat to the plant.

Of paramount importance in the proposed control strategy is the assumption that the HTF leaving the power block has a constant temperature and it is different from

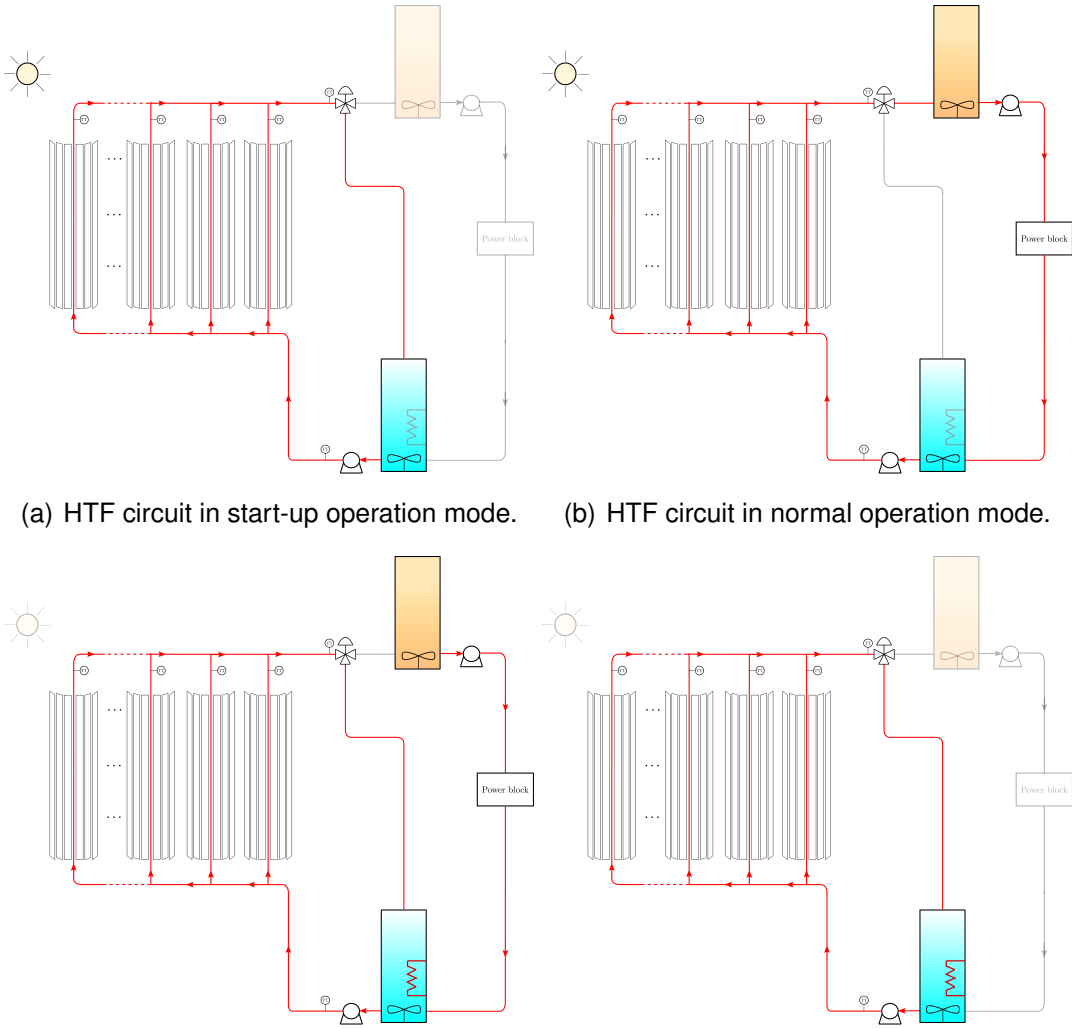

(a) HTF circuit in start-up operation mode.

(b) HTF circuit in normal operation mode.

(c) HTF circuit in shut-down operation mode.

(d) HTF circuit in night and anti-freeze operation mode.

Figure 5 – Schematic diagrams of the operation modes of the CSP plant.

that one entering the power block. From a practical point of view, this assumption is reasonable when the power block is working at the nominal operating mode and allows to decouple the temperature dynamics of the hot TES system with respect to the one of the solar collector field.

2.2 MATHEMATICAL MODEL

Any model of CSP plants must take into account the relationships between radiation availability, HTF thermodynamic properties, heat losses and mass conservation inside the system, besides the couplings between the subsystems involved in the whole process. Bearing in mind these principles, a general model for describing the states of the plant can be developed. In this section, the main equations needed for the optimal control design will be presented briefly. The interested reader is referred to E.F. Camacho et al. (2012) and Egeland and Gravdahl (2002) for more details on the modeling

assumptions and simplifications.

2.2.1 Heat Transfer Fluid

According to Lopes et al. (2020), the thermodynamic properties of the molten salts satisfy the following equations with a coefficient R^2 greater than 0.99:

$$h(T) = 1435.5\,T + 422740, \tag{1}$$

$$\rho(T) = 2240 - 0.8266\,T, \tag{2}$$

$$c_p(T) = 1546.2 - 0.3\,T. \tag{3}$$

In (1)-(3), h is the specific enthalpy [J/kg], ρ represents the specific mass [kg/m^3], c_p is the specific heat [J/kg °C] and T is the temperature [°C].

In the next sections, the notation h_i, ρ_i and $c_{p,i}$ is used to represent the thermodynamic property of the HTF in the subsystem i calculated from its temperature, T_i.

2.2.2 Solar Collector Field

In this work, a lumped-parameter physical model, which was obtained from the nonlinear PDE presented in E.F. Camacho et al. (2012), is considered to describe the temperature dynamics of the solar collector field. This model was arrived at by removing the dependence on space in the original model. It also considers that the heat flow in the solar field is radially uniform and equal to the average flow; the temperature variation of the absorber tube walls is negligible; solar radiation is a function of time only; and specific heat at constant pressure and volume are equivalent. Thus, applying the energy conservation law, the following equation is obtained:

$$\rho_c\, c_{p,c}\, A_e\, \frac{dT_c}{dt} = \alpha_{op}\, \gamma\, G\, I - \frac{c_{p,c}\, m_c\, (T_c - T_{tf})}{\eta\, S_{loop}} - \frac{\tilde{H}_l\,(T_m,\, T_{amb})}{S_c}, \tag{4}$$

where (variable arguments have been omitted for readability) $t \in [0, \infty)$ denotes the time, T_c (controlled variable) is the outlet temperature [°C], T_{tf} is the inlet temperature [°C] – which is given by the outlet temperature of the cold TES system (see Figure 4) –, T_m is the average between T_c and T_{tf}, and T_{amb} is the ambient temperature [°C]. The outlet mass flow rate [kg/s] is given by $m_c \in [m_c^{min},\, m_c^{max}]$ (control variable), with $0 < m_c^{min} < m_c^{max}$, while the specific mass [kg/m^3] and specific heat [J/(kg °C)], both computed from T_c, are given by ρ_c and $c_{p,c}$, respectively. The solar radiation [W/m^2] is given by I, the collector optical efficiency (more details presented in Section 2.2.2.1 and 2.2.2.2) is given by $\alpha_{op} \in [0,\, \alpha_{op}^{max}]$, where $\alpha_{op}^{max} \in (0,\, 1]$, its aperture [m] is given by G and $\gamma \in [0,\, 1]$ represents the defocus of the collectors (control variable). The pipe cross-section area [m^2] is denoted by A_e, the length of the loop [m] is given by S_{loop},

the number of loops is η and S_c denotes the total length of the solar collector field [m]. The term $\tilde{H}_l$ [J/s] represents the thermal losses by convection. Some of these variables are presented in Figure 6.

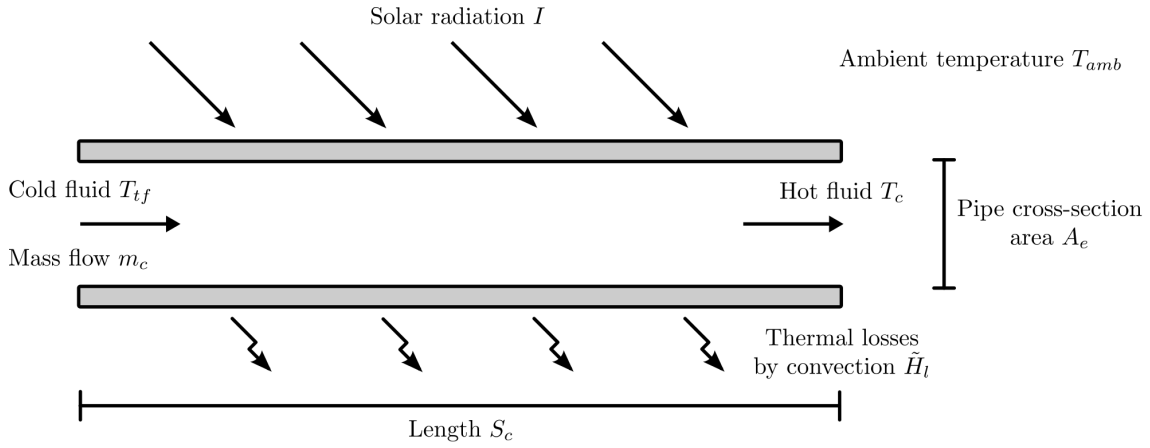

Figure 6 – Representation of the absorber tube in the solar field.

Assumption 1. *The term $\tilde{H}_l$ in (4) is assumed to be a first order polynomial in T_m and T_{amb}.*

The initial condition of (4) is $T_c(0) = T_c^0$, with $T_c^0 \in \mathbb{R}$.

Assumption 2. *The initial condition, T_c^0, of (4) verifies $T_c^0 \leq T_{tf}(0)$.*

Additionally, in this work it is defined that the physical parameters of (4) satisfy the following conditions:

Assumption 3. *For the entire region of operation of the plant, the system coefficients verify the following inequality:*

$$\frac{c_{p,c}\, m_c\, (T_{tf} - T_c)}{\eta\, S_{loop}} - \frac{\tilde{H}_l\, (T_m, T_{amb})}{S_c} < 0$$

Note that Assumption 3 indicates that during the night the collector field is mainly influenced by losses due to convection with the environment.

To determine model (4) more precisely, the varying pattern of I is now specified. Let $t \in [0, t_f]$ be the time interval of one day, where t_f is the duration of the day. Then, define the subintervals $[0, t_N]$, $(t_N, t_D]$, $(t_D, t_f]$, with $0 < t_N < t_D < t_f$, and such that $[0, t_N] \cup (t_N, t_D] \cup (t_D, t_f] = [0, t_f]$. The subinterval $[0, t_N]$ is denoted as the first night period of the day, $(t_N, t_D]$ as the day interval, and $(t_N, t_D]$ as the second night period of the day, as can be seen in Figure 7. Note that at the equinox, $\frac{t_D - t_N}{2} = \frac{t_N + (t_f - t_D)}{2}$, but obviously this will depend on the time of the year.

Thus, solar radiation is described as follows

$$I(t) = \begin{cases} s(t), & \text{if } t \in (t_N, t_D], \\ 0, & \text{if } t \in [0, t_N] \text{ or } t \in (t_D, t_f], \end{cases} \tag{5}$$

in which $s : (t_N, t_D] \rightarrow \mathbb{R}_+$ is a function that describes the variation in solar radiation during the day such that $I_{min} \leq s(t) \leq I_{max}\ \forall t \in (t_N, t_D]$, with $0 < I_{min} < I_{max}$.

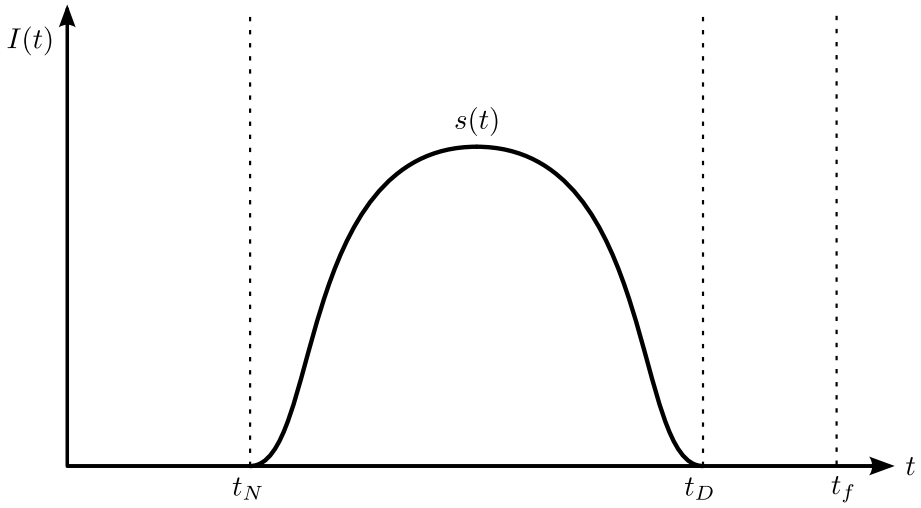

Figure 7 – Solar radiation description.

2.2.2.1 Solar Position

In order to obtain the optical efficiency, α_{op}, of the linear Fresnel solar collector, it is necessary to generate values of transverse and longitudinal incidence angles in the plant. The Solar Position Algorithm (SPA) is implemented using MATLAB software and it calculates the solar zenith and azimuth angles in for any time period between the year -2000 to 6000, with uncertainties of +/- 0.0003 degrees based on the date, time, and location on Earth (REDA; ANDREAS, 2004). The *PV_LIB Toolbox* with function *pvl_spa* implements a vectorized version of NREL's SPA.

The topocentric zenith angle is

$$\theta_{ze} = 90^{\circ} - arcsin\left(sin\left(\theta_{gl}\right) sin\left(\theta_{de}\right) + cos\left(\theta_{gl}\right) cos\left(\theta_{de}\right) cos\left(\theta_{hr}\right)\right) - \Delta, \qquad (6)$$

in which θ_i, for $i \in \{de, hr, gl\}$, are angles represented in degrees. The sub-index de denotes the topocentric sun declination, which represents the angle between the Earth's axis of rotation and the plane normal to a line connecting the centers of the Earth and Sun, and hr is the topocentric local hour angle and corresponds the angle of the Sun in its apparent orbit through the sky. By convention it is defined to zero at solar noon (when the Sun reaches its highest point in the sky each day). The geocentric latitude of the observer is represented by the sub-index gl. Δ is the correction of atmospheric refraction (in degrees) and depends on the annual average local pressure (in millibars), the annual average local temperature [ºC] and the topocentric elevation angle (in degrees). The atmospheric refraction term is an optional function and is not implemented due to lack of local pressure data.

The topocentric azimuth angle is calculated by

$$\theta_{az} = arctan\,2\left(\frac{sin\,(\theta_{hr})}{cos\,(\theta_{hr})\,sin\,(\theta_{gl}) - tan\,(\theta_{de})\,cos\,(\theta_{gl})}\right) - \theta_{az,c}, \tag{7}$$

where $\theta_{az,c}$ is the azimuth angle position of the solar collector field and $arctan\,2$ is a function that returns the four-quadrant inverse tangent in the closed interval $[-\pi, \pi]$. In contrast, $arctan$ returns results that are limited to the interval $[-\pi/2, \pi/2]$.

Using the topocentric sun declination, topocentric local hour and the geocentric latitude of the observer, calculated based on their geographic position (latitude and longitude in degrees), altitude (meters) and the day of solar incidence, it is possible to calculate the topocentric zenith angle (6) and topocentric azimuth angle (7), as can be seen in Figure 8. Therefore, using θ_{ze} and θ_{az} it is possible to obtain the incidence angles in the solar collector field by

$$\sigma_{tr} = arctan\,(tan\,(\theta_{ze})\,sin\,(\theta_{az}))\,\frac{\pi}{180},$$
$$\sigma_{lo} = arctan\,(tan\,(\theta_{ze})\,cos\,(\theta_{az}))\,\frac{\pi}{180},$$

in which σ_i is in radians for $i \in \{tr,\, lo\}$ and the sub-index tr represents the transversal and lo the longitudinal incident angles.

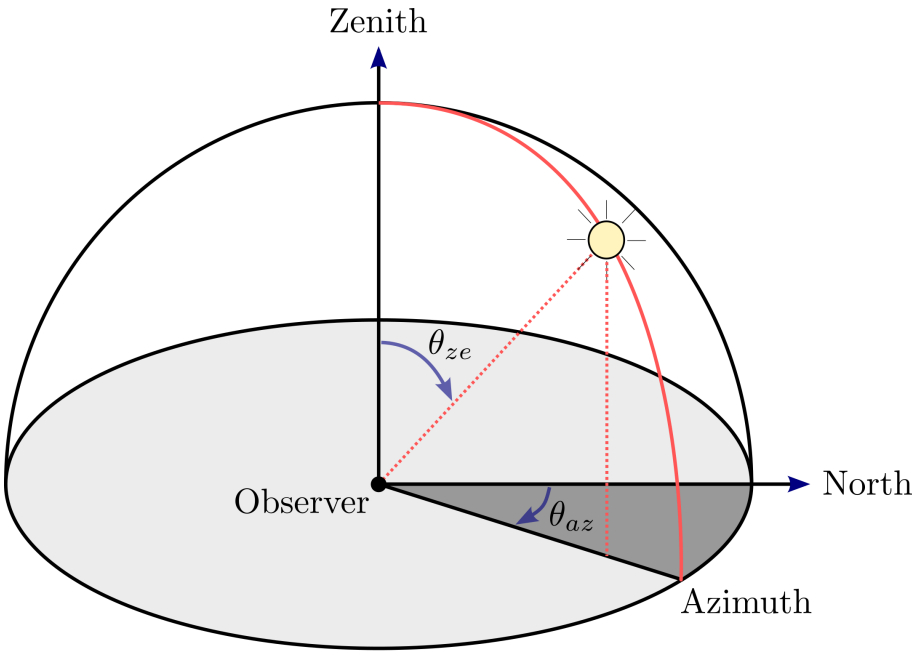

Figure 8 – Zenith and Azimuth angle of Solar position.

2.2.2.2 Optical Efficiency

The Incident Angle Modifier (IAM) allows to calculate the optical efficiency variations due to deviation of the Sun in transversal and longitudinal incident angle directions. This optical efficiency multiplied by the direct normal irradiance $I(t)$ aims to calculate

the heat flux on the absorber tube at a given point in time for a linear Fresnel solar collector.

Table 1 – Incident angle modifier for the FRENELL DMS linear Fresnel solar collector technology.

Angle (°)	Transversal IAM	Longitudinal IAM
0	1	1
10	0.98	0.98
20	0.96	0.92
30	0.95	0.83
40	0.91	0.69
50	0.86	0.52
60	0.70	0.31
70	0.48	0.11
80	0.23	0
90	0	0

The IAMs functions are calculated based on a linear interpolations of the respective collector IAM data described in Table 1 (BACHELIER; STIEGLITZ, 2017). Interpolating data allows one to obtain the following transversal IAM polynomial and longitudinal IAM polynomial:

$$IAM_{tr}(\sigma_{tr}) = -0.2320\,|\sigma_{tr}|^3 - 0.0813\,|\sigma_{tr}|^2 + 0.0546\,|\sigma_{tr}| + 0.9844,$$
$$IAM_{lo}(\sigma_{lo}) = 0.6484\,|\tau_{lo}|^4 - 1.3710\,|\tau_{lo}|^3 + 0.2602\,|\sigma_{lo}|^2 - 0.1769\,|\sigma_{lo}| + 1.0025,$$

and the optical efficiency is now given by

$$\alpha_{op}(\sigma_{tr}, \sigma_{lo}) = IAM_{tr}\,(\sigma_{tr})\;IAM_{lo}\,(\sigma_{lo})\;SW\,DM\,EM,$$

in which SW is the solar-weighted mirror reflectivity value, DM is the dirt on mirror derate and EM is the general optical error derate.

2.2.3 Thermal Energy Storage

The storage tanks are of the vertical cylindrical type with a flat bottom. It is assumed that these tanks are operating at ambient pressure and the same temperature throughout the volume, that is, perfect mixture. The other considerations are similar to those of the solar field presented in the previous section. Thus, the following mass balances are satisfied (EGELAND; GRAVDAHL, 2002):

$$A_{tq}\,\rho_{tq}\,\frac{dL_{tq}}{dt} = m_c\,\beta - m_p, \tag{8}$$
$$A_{tf}\,\rho_{tf}\,\frac{dL_{tf}}{dt} = m_p - m_c\,\beta, \tag{9}$$

where the sub-indices tq and tf represent the variables of the hot and cold TES systems, respectively. For $i \in \{tq, tf\}$, L_i represents the liquid level [m] of the tank i and A_i

represents its cross-sectional area [m^2]. The outlet mass flow rate [kg/s] of the hot TES system is $m_p \in [0,\, m_p^{max}]$ (control variable), with $m_p^{max} > 0$, at the same time m_p is the mass flow rate from the power block to the cold fluid TES system[1]. The outlet mass flow rate [kg/s] of the cold TES system is given by m_c. β represents a Boolean function, that is, $\beta : \mathbb{R} \to \{0, 1\}$, and is used to impose the plant's mode of operation according to the description in Section 2.1.1.

Assumption 4. *For the system under consideration, the inequality* $m_c^{max} > m_p^{max}$ *holds.*

Assumption 4 indicates that the plant is over sized (solar multiple greater than 1), that is, it is possible to generate more energy with the solar receiver than the power block can transform. This indicates that the system can continue to operate when TES system is the only source of energy.

The initial conditions of (8)-(9) are $L_{tq}(0) = 0$ and $L_{tf}(0) = L_{tf}^0$, with $L_{tf}^0 \in \mathbb{R}_+$. From (8), it is obtained that

$$L_{tq}(t) = \frac{1}{A_{tq}} \int_0^t \frac{1}{\rho_{tq}} \left(m_c\, \beta - m_p\right) d\tau.$$

So, it follows that

$$\frac{1}{A_{tq}\, \rho_{tq}^{min}} \left(m_c^{max} - m_p^{max}\right) t \leq L_{tq}(t) \leq \frac{1}{A_{tq}\, \rho_{tq}^{min}}\, m_c^{max}\, t. \tag{10}$$

The Inequalities in (10) give us an upper and lower elevation for the liquid level in the hot TES as a function of the maximum mass flow of the solar field and the power block, respectively. From a practical point of view, the volume of the TES and the nominal point of operation of the solar field must be properly dimensioned so that system saturation does not occur. The greater the ratio between the mass flow from the solar field and the discharge flow to the power block, the greater the volume of the hot TES must be.

To describe the temperature of the heat transfer fluid in the storage tanks, it is used that the specific enthalpy can be written

$$h_i = \frac{H_i}{\rho_i\, A_i\, L_i},$$

where the H_i is the enthalpy of the system. Knowing that the area of the tank is constant,

[1] It is important to emphasize that the power block dynamics were neglected in this work. In this way, it is assumed that the power block outlet temperature is constant and equal to its nominal operating value.

it is possible to develop the equation of enthalpy as being

$$\begin{aligned}\frac{dH_i}{dt} &= \frac{d}{dt}\left(h_i\,\rho_i\,A_i\,L_i\right) = A_i\,\frac{d}{dt}\left(h_i\,\rho_i\,L_i\right) = A_i\left[h_i\,\rho_i\,\frac{dL_i}{dt} + L_i\,\frac{d\rho_i h_i}{dt}\right] \\ &= A_i\left[h_i\,\rho_i\,\frac{dL_i}{dt} + L_i\,h_i\,\frac{d\rho_i}{dT}\,\frac{dT_i}{dt} + L_i\,\rho_i\,\frac{dh_i}{dT}\,\frac{dT_i}{dt}\right] \\ &= A_i\left[h_i\,\rho_i\,\frac{dL_i}{dt} + L_i\,\frac{dT_i}{dt}\left(h_i\,\frac{d\rho_i}{dT} + \rho_i\,\frac{dh_i}{dT}\right)\right]. \end{aligned} \tag{11}$$

Combining the enthalpy (11) with the mass balance in the storage tanks (8) and (9), then the enthalpy of the storage tanks can be written as

$$\frac{dH_{tq}}{dt} = A_{tq}\left[h_{tq}\,\rho_{tq}\,\frac{m_c\,\beta - m_p}{\rho_{tq}\,A_{tq}} + L_{tq}\,\frac{dT_{tq}}{dt}\left(h_{tq}\,\frac{d\rho_{tq}}{dT_{tq}} + \rho_{tq}\,\frac{dh_{tq}}{dT_{tq}}\right)\right], \tag{12}$$

$$\frac{dH_{tf}}{dt} = A_{tf}\left[h_{tf}\,\rho_{tf}\,\frac{m_p - m_c\,\beta}{\rho_{tf}\,A_{tf}} + L_{tf}\,\frac{dT_{tf}}{dt}\left(h_{tf}\,\frac{d\rho_{tf}}{dT_{tf}} + \rho_{tf}\,\frac{dh_{tf}}{dT_{tf}}\right)\right]. \tag{13}$$

Using the energy balance of the tanks

$$\begin{aligned}\frac{dH_{tq}}{dt} &= m_c\,\beta\,h_c - m_p\,h_{tq} - \tilde{P}_l, \\ \frac{dH_{tf}}{dt} &= m_c\,(1-\beta)\,h_c + m_p\,h_p - m_c\,h_{tf} - \tilde{P}_l + Q,\end{aligned}$$

and adding in the enthalpy equation of the tanks (12)(13), respectively, the following temperature equations of the heat transfer fluid in the storage tanks it is obtained

$$\begin{aligned}L_{tq}\,A_{tq}\left(h_{tq}\frac{d\rho_{tq}}{dT_{tq}} + \rho_{tq}\frac{dh_{tq}}{dT_{tq}}\right)\frac{dT_{tq}}{dt} = {}& m_c\,\beta\left(h_c - h_{tq}\right) \\ & - \tilde{P}_l\left(T_{tq} - T_{amb}\right), \end{aligned} \tag{14}$$

$$\begin{aligned}L_{tf}\,A_{tf}\left(h_{tf}\frac{d\rho_{tf}}{dT_{tf}} + \rho_{tf}\frac{dh_{tf}}{dT_{tf}}\right)\frac{dT_{tf}}{dt} = {}& \\ m_c\,(1-\beta)\left(h_c - h_{tf}\right) + m_p\left(h_p - h_{tf}\right) & \\ - \tilde{P}_l\left(T_{tf} - T_{amb}\right) + Q, & \end{aligned} \tag{15}$$

for $i \in \{tq,\, tf\}$, T_i is the temperature [°C] of the fluid in the tank i, being T_{tf} a controlled variable, and $Q \in [0,\, Q^{max}]$, with Q^{max}, represents the heat [W] released by the electrical resistance (control variable) in the cold TES system. The specific enthalpy [J/kg] of output from the solar collector field is given by h_c and the specific enthalpy [J/kg] of output from the power block is given by h_p. The term $\tilde{P}_l$ [kJ/s] is the coefficient of thermal losses of the tanks by convection and it is assumed to be a positive constant. The complete TES system can be seen in Figure 9.

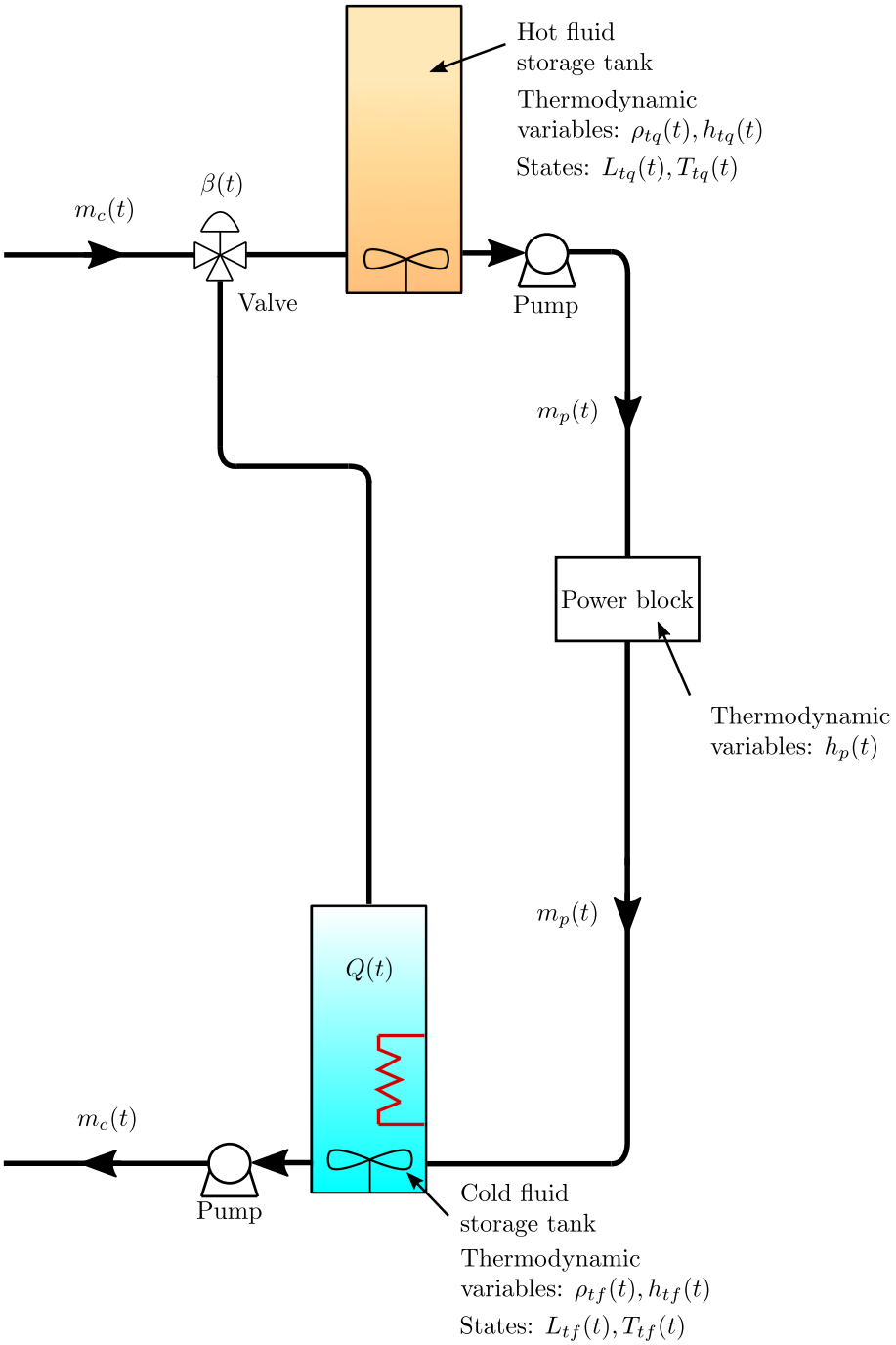

Figure 9 – TES system.

The initial conditions of (14)-(15) is $T_{tq}(0) = T_{tq}^0$ and $T_{tf}(0) = T_{tf}^0$, respectively, with $T_{tq}^0, T_{tf}^0 \in \mathbb{R}$.

Assumption 5. *Regarding the initial conditions of* (14)-(15)*, it was assumed that* $T_{tq}^0 > T_{tf}^0$.

2.3 CONTROL PROBLEM

Since the storage unit completely decouples the power block from the solar energy source, the CSP plant control problem can be divided into two subproblems: (i)

the solar collector field control problem; and (ii) the dispatch of the hot TES system to the power block.

The control objective in the solar collector field is to maintain its outlet temperature around the desired reference value. The solar radiation cannot be manipulated, so the temperature control is performed by changing the HTF mass flow rate through the solar field. The main disturbances are the changes in the HTF inlet temperature, variations in the ambient temperature, changes in the optical coefficient – resulting from the solar position and the reflection of the mirrors – and changes in solar radiation due to the daily cycle or passing clouds. Importantly, the controller must handle the maximum power that can be manipulated by the receiver by partially defocusing the mirrors.

On the other hand, the dispatch control problem aims to maximize the daily revenue from the electricity sales by manipulating the outlet mass flow rate of the hot TES system. In order to ensure a feasible operation, the control system must avoid the power block operation below a minimum load and fast changes and oscillations of the mass flow rate, as well as repeated re-starts of the plant during the same day. This controller must also ensure that the HTF in the cold TES system remains around the desired temperature reference to prevent its freezing during the night. This is accomplished by manipulating the electrical resistance located in this tank.

3 OPTIMAL CONTROL

In the previous chapter, the control objective was presented, working principle and mathematical model of the solar plant. Next, the Optimal Control Strategy proposed in this work will be presented. In this context, a basic material on optimal control focusing mainly on indirect and direct resolution approaches is presented. This material has been extracted from references Liberzon (2012), Athans and Falb (2007) and Betts (2010). Then, the problem of optimal control of the solar plant is formulated and analyzed. In particular, the behavior of the solution is verified through the Pontryagin's Maximum Principle characterizing the nature of the ideal solution. The practical implementation of the controller through a direct approach is also proposed and discussed in this chapter.

3.1 BASIC MATERIAL

The objective of optimal control theory is to determine the control signals that will cause a process to satisfy some constraints and at the same time minimize (or maximize) some performance criterion. It has several applications in engineering, such as, train control (HOWLETT et al., 2009), sensor scheduling (WU et al., 2020), hybrid electric vehicle (SCIARRETTA et al., 2004), and hybrid power systems (LIN; ZHENG, 2011). The advantages of a control system based on the optimal control theory stands out when it comes to multiple-input multiple-output systems, where traditional performance measures such as settling time, static gain and phase margin may be inadequate for describing the desired behavior. There are various types of Optimal Control Problems (OCPs), depending on the performance index, the type of time domain (continuous, discrete), the presence of different types of constraints, and what variables are free to be chosen. The interested reader is referred to Athans and Falb (2007) for more details. In this section, the basic concepts of a particular case of an OCP will be discussed.

The basic OCP under consideration is represented as follows:

$$
\begin{aligned}
&\min_{u(.)} \quad \int_0^{t_f} J(t, x(t), u(t))dt, \\
&\text{s. t.:} \\
&\qquad x(0) = x_0, \\
&\qquad \dot{x}(t) = f(t, x(t), u(t)), \quad \forall t \in [t_0, t_f], \\
&\qquad g(t, x(t), u(t)) \leq 0, \qquad \forall t \in [t_0, t_f],
\end{aligned}
\tag{16}
$$

in which x is the state taking values in $\mathbb{R}^n$, u is the control variable taking values in some control set $U \subset \mathbb{R}^m$, $t \in [0,\, t_f]$ is the time, where $t_f > 0$ is the final time assumed to be fixed and known. The running cost is given by $J : [0,\, t_f] \times \mathbb{R}^n \times \mathbb{R}^m \to \mathbb{R}$, $x_0 \in \mathbb{R}^n$ is the initial value condition, and $f : [0,\, t_f] \times \mathbb{R}^n \times \mathbb{R}^m \to \mathbb{R}^n$ is a given vector valued function. Finally, $g : [0,\, t_f] \times \mathbb{R}^n \times \mathbb{R}^m \to \mathbb{R}^v$ is the inequality path constraints.

Basically, there are three classes of methods for solving (16): (i) continuous time dynamic programming; (ii) indirect methods; and (iii) direct methods.

Continuous time dynamic programming is based on solving the Hamilton-Jacobi-Bellman equation, which is a partial differential equation (LEEK, 2016). The advantages of this approach is that it provides sufficient conditions for optimality and in some cases the optimal control law can be expressed explicitly. For example, for linear dynamical systems, the Hamilton-Jacobi-Bellman equation degenerates into a Riccati equation, which is very easy to solve. However, for the most nonlinear cases, the Hamilton-Jacobi-Bellman partial differential equation is hard to solve analytically and numerically for the solar power plant problem.

Indirect methods are based on the Pontryagin's maximum principle (PMP), which is a powerful method for solving optimization problems because it has the important advantage of not requiring the evaluation of the payoff functional (LIBERZON, 2012). In particular, the PMP transforms the problem (16) into a Boundary Value Problem (BVP) and the optimal trajectories are obtained by solving this BVP, which requires the use of mathematical tools much less advanced than other approaches. These methods have a very well established theory and can be computationally efficient in many cases. The reader interested in some applications of the PMP is referred to Bonvin and Srinivasan (2013).

Finally, direct methods discretize the system states and/or the control inputs of the OCP in order to transform it into a Nonlinear programming (NLP) problem, which can be solved by using well-known nonlinear optimization algorithms and high-speed computers.

3.2 PONTRYAGIN'S MAXIMUM PRINCIPLE

The Pontryagin's Maximum Principle can be described as a collection of conditions that must be satisfied by the solution of (16). It unifies many classical necessary conditions from the calculus of variations and was formulated by Lev Pontryagin to solve the maximization problem of the terminal speed of a rocket (GAMBKRELIDZE, 1999). Its main advantage lies in the fact that maximizing (resp. minimizing) the Hamiltonian of the problem is much easier than the original control problem. In this section, these conditions will be briefly presented.

Let the Hamiltonian of (16) be defined as

$$\mathcal{H}(t, x, u, \lambda) := \langle \lambda, f(t, x, u) \rangle + J(t, x, u). \tag{17}$$

where $\lambda : [0, t_f] \to \mathbb{R}^n$ is the costate and $\langle \cdot, \cdot \rangle$ denotes the internal product.

The Lagrangian with constraints directly adjoined is

$$\mathcal{L}(t, x, u, \lambda, \mu) := \mathcal{H}(t, x, u, \lambda) + \langle \mu, g(t, x(t), u(t)) \rangle , \tag{18}$$

where $\mu : [0, t_f] \to \mathbb{R}^v$ are the Lagrange multipliers.

Let x^{opt} and u^{opt} denote a local minimum pair of the OCP (16). Then, according to Clarke and De Pinho (2010) there exists a piecewise continuous costate λ^{opt} and piecewise continuous multipliers μ^{opt} such that the following conditions hold:

1. Adjoint equations

$$\lambda^{opt}(t) = -\frac{\partial}{\partial x}\mathcal{L}(t, x^{opt}, u^{opt}, \lambda^{opt}, \mu^{opt}), \tag{19}$$

$$\lambda^{opt}(t_f) = 0; \tag{20}$$

2. maximum (resp. minimum) condition for the standard Hamiltonian

$$\mathcal{H}(t, x^{opt}, u^{opt}, \lambda^{opt}) = \max_{u(t)} \mathcal{H}(t, x^{opt}, u, \lambda^{opt}); \tag{21}$$

3. local maximum (resp. minimum) condition for the Lagrangian

$$\frac{\partial}{\partial u}\mathcal{H}(t, x^{opt}, u^{opt}, \lambda^{opt}) = 0; \tag{22}$$

4. complementary condition

$$\mu^{opt} \geq 0, \qquad \mu^{opt} h(t, x^{opt}, u^{opt}) = 0. \tag{23}$$

It is important to note that (19)-(23) are necessary conditions for the problem (16). Trajectories satisfying these conditions are called extremals and one way to think of the Maximum Principle is as identifying a subset of controlled trajectories as being candidates for optimality. Sometimes this restricted candidacy is enough to actually characterize the optimal trajectories. In other cases, it can turn out that much additional work needs to be done beyond the Maximum Principle to distinguish the optimal trajectories from the extremals.

3.3 DIRECT OPTIMAL CONTROL

Direct methods for optimal control, also known as *first-discretize-then-optimize* approaches, are based on numerical solutions (QUIRYNEN, 2017). The discretization can be divided in three fundamental steps (BETTS, 2010):

- convert the dynamic system into a problem with a finite set of variables;
- solve the finite-dimensional problem using a parameter optimization method (i.e., the NLP subproblem);
- assess the accuracy of the finite-dimensional approximation and if necessary repeat the transcription and optimization steps.

Considering these steps, it is convenient to view the original OCP as an infinite-dimensional extension of an NLP problem, since the OCP involves continuous functions, such as $x(t)$ and $u(t)$, and the NLP problem is characterized by a finite set of variables and constraints.

The direct method is essentially divided in three different forms, namely direct single shooting, direct multiple shooting and direct collocation, which differ in the process of transforming the continuous part of the OCP into a NLP. The multiple shooting method is often superior to the other methods since it presents faster convergence properties, stronger flexibility in initializing the problem, where the user can initialize with a known guess for the state trajectory, and parallelizing the algorithm since the optimization and simulation problems are solved together (ALBERSMEYER; DIEHL, 2010, 2010). The drawback is that the NLP gets much larger, although this is often compensated by the fact that the problem becomes sparse.

3.3.1 Multiple Shooting Parameterization

The direct multiple shooting method, proposed by Bock et al. (1987) and Bock and Plitt (1984), is a numerical method for the solution of boundary value problems. The key idea of multiple shooting method is to break down the system integration into short time intervals, i.e., to consider the system model equations as equatility constraints to ensure continuity of the trajectory at each optimization step $s_{i+1} - x_i(t_{i+1}; s_i, q_i) = 0$, and consequently, the states will become decision variables in the optimization problem as well as control variables $w = [x_0, \cdots, x_i, u_0, \cdots, u_{i-1}]$. The terms s and q will be covered later.

The main steps for the direct multiple shooting parameterization are the following.

Multiple shooting grid: The fundamental idea is to discretize the time domain $I = [0, t_f]$ into $N - 1$, with $N \in \mathbb{N}$, subintervals $I_i := [t_i, t_{i+1}]$, such that

$$0 = t_0 < t_1 < \cdots < t_N = t_f.$$

Mathematically, the time interval $t \in [0, t_f]$ is divided into N equidistant segments of length (stepsize), T_s, with

$$T_s = \frac{t_f}{N},$$

and

$$\begin{aligned} t_0 &= 0, \\ t_{i+1} &= t_i + T_s, \quad i \in \{0, 1, \ldots, N-1\}. \end{aligned}$$

Control parameterization: On each subinterval the control trajectory $u(t)\ \forall t \in [0, t_f]$ is parameterized by a finite number of parameters which yield a suitable approximation, i.e.,

$$u(t) = q_i, \quad \text{for} \quad t \in [t_i, t_{i+1}], \quad i \in \{0, 1, \ldots, N-1\},$$

with N local control parameter vectors $q_0, q_1, \ldots, q_{N-1}$, $q_i \in \mathbb{R}^m$.

State parameterization: Direct multiple shooting method introduces additional state variables s_i on the grid points in order to explicitly couple the IVPs. On each subinterval the initial condition of the state vector $x(t_i)$ is parameterized as

$$x(t_i) = s_i, \qquad i \in \{0, 1, \ldots, N\},$$

with $N+1$ local states vectors $s_0, s_1, \ldots, s_N$, $s_i \in \mathbb{R}^n$ and all but the last serve as initial values for N independent IVPs on the subintervals I_i. The ODE on each subintervals $[t_i, t_{i+1}]$ is then solved independently, starting with an artificial initial value s_i

$$\begin{aligned} \dot{x}_i(t) &= f(t, x_i(t), q_i), \quad t \in [t_i, t_{i+1}], \\ x_i(t_i) &= s_i. \end{aligned}$$

In general, analytic propagation is not feasible and numerical methods must be employed. The numerical solution of the IVP for ODEs is fundamental to most optimal control methods. The differential equations can be discretized using a Runge Kutta 4th (RK4) order scheme:

$$x_i(t; s_i, q_i) := x_{i+1} = x_i + \int_{t_i}^{t_{i+1}} f(t, x_i(t), q_i) dt,$$

into

$$x_{i+1} = x_i + \frac{T_s}{6}(k_1 + 2k_2 + 2k_3 + k_4), \tag{24}$$

with

$$\begin{aligned} k_1 &= f(x_i, q_i), \\ k_2 &= f(x_i + \frac{T_s}{2} k_1, q_i), \\ k_3 &= f(x_i + \frac{T_s}{2} k_2, q_i), \\ k_4 &= f(x_i + T_s k_3, q_i). \end{aligned}$$

The numerical solution of these IVPs are N independent trajectories $x_i(t)$ on $[t_i, t_{i+1}]$, which are a function of s_i and q_i only. The state variables on every subinterval are replaced by the computed solution $x_i(t; s_i, q_i)$, where the extra arguments after the semicolon are introduced to denote the dependence on the interval's initial values and controls (see Figure 10). The decoupled IVPs are connected by matching conditions requiring that each node value equals the final value of the preceding trajectory. To ensure the state trajectory to be continuous the following constraint is formed

$$s_{i+1} - x_i(t_{i+1}; s_i, q_i) = 0, \quad i = 0, 1, \ldots, N-1. \tag{25}$$

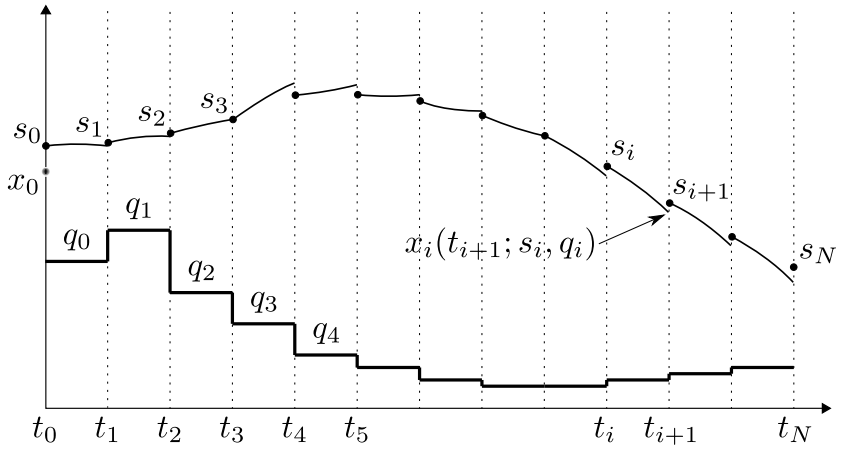

Figure 10 – Numerical integrators build the simulations $x_i(t, s_i, q_i)$ over each time interval $[t_i, t_{i+1}]$. The state trajectory held in the NLP solver becomes continuous only when the solution of the NLP is reached, where the continuity conditions $s_{i+1} - x_i(t_{i+1}, s_i, q_i) = 0$ are enforced.

NLP formulation: To arrive at the finite dimensional NLP approximation of (16), the continuous time objective function also must be discretized:

$$\int_{t_0}^{t_f} J(t, x(t), u(t))dt \approx \sum_{i=0}^{N-1} J_i(s_i, q_i). \tag{26}$$

that is,

$$J_i(s_i, q_i) := \int_{t_i}^{t_{i+1}} J(t, x_i(t; s_i, q_i), q_i)dt.$$

Then, the NLP formulation of the OCP (16) is given by

$$\begin{aligned} \min_{s_i, q_i} \quad & \sum_{i=0}^{N-1} J_i(s_i, q_i) \\ \text{s. t.:} \quad & \\ & s_0 - x(0) = 0, \\ & s_{i+1} - x_i(t_{i+1}, s_i, q_i) = 0, \qquad i = 0, 1, \ldots, N-1, \\ & g(s_i, q_i) \leq 0, \qquad\qquad\quad i = 0, 1, \ldots, N-1. \end{aligned} \tag{27}$$

3.3.2 CasADi: A tool for solving nonlinear programming problems

In this dissertation, the OCPs studied will be solved numerically using the CasADI software. CasADi is an open-source software framework for numerical optimization and started out as a tool for Algorithmic Differentiation (AD) using a syntax similar to a Computer-algebra System (CAS), explaining its name. The AD is still a key feature of CasADi, but the focus has since shifted towards optimization, computation of initial value problems in Ordinary Differential Equations (ODEs) or differential-algebraic

equations, quadratic programming, NLP and interfaces to other numerical tools. CasADi provides a set of building blocks that drastically decreases the effort needed to implement a large set of algorithms for numerical optimal control, without sacrificing efficiency (ANDERSSON et al., 2019). Although it is written in self-contained C++ programming language, it can be used full-featured interfaces to Python, MATLAB or Octave.

3.4 OPTIMAL CONTROL APPLIED TO THE SOLAR POWER PLANT

In this section, the optimal control theory is applied to the solar power plant control problem described in Section 2.3. The approach to solving the problem is decentralized thanks to the decoupling between the outlet temperature of the hot TES system and the inlet temperature of the solar collector field. In this context, the reference tracking and disturbances rejection problem in the solar collector field, i.e., problem (i) described in Section 2.3, is firstly formulated and solved for a fixed time interval $[0, t_f]$. The optimal and control state trajectories obtained from the solution of this problem are then fed into the control problem (ii), which is solved for the same fixed time interval $[0, t_f]$ in order to compute the control policy for the control variables of the TES systems. This design is detailed in what follows.

3.4.1 Solar Collector Field

Let $U_0 = (\gamma,\ m_c,\ \beta)$ be the vector of control variables. Then, the following continuous time optimization problem is formulated for $t \in [0,\ t_f]$, with t_f a fixed value:

$$
\begin{aligned}
P_0: \quad & \min_{U_0(t) \in \mathcal{U}_0} \int_0^{t_f} \Big(c_0 \left(T_{c,ref} - T_c\right)^2 + c_1\, m_c^2 \\
& \qquad\qquad -\alpha_{op}\, \gamma\, G\, I + \beta \left(T_{c,rec} - T_c\right) \Big) dt, \\
\text{s. t.:} \quad & \\
& \rho_c\, c_{p,c}\, A_e \tfrac{dT_c}{dt} = \alpha_{op}\, \gamma\, G\, I - \tfrac{c_{p,c}\, m_c\, (T_c - T_{tf})}{\eta\, S_{loop}} \\
& \qquad\qquad - \tfrac{\tilde{H}_l\, (T_m, T_{amb})}{S_c}, \\
& T_c(0) = T_c^0,
\end{aligned}
\tag{28}
$$

in which

$$
\begin{aligned}
\mathcal{U}_0 = \{(\gamma,\ m_c,\ \beta) \in \mathbb{R}^3 \mid\ & 0 \leq \alpha_{op}\, \gamma\, G\, I \leq \alpha_{op,max}\, G\, I_{max}, \\
& m_{c,min} \leq m_c \leq m_{c,max},\ 0 \leq \beta \leq 1\}.
\end{aligned}
$$

In (28), the term $T_{c,ref} \in \mathbb{R}$ denotes the outlet reference temperature [°C] of the solar collector field in nominal operating mode, $T_{c,rec} \in \mathbb{R}$ is the temperature value to switch between the start-up and nominal operating modes (see Section 2.1), and $c_0 > 0$ and $c_1 \geq 0$ are design constants.

The first term in the functional in (28) is responsible for tracking the reference temperature of the solar field, while the second term is introduced to penalize rapid variations in mass flow rate. The third term in the functional in (28), together with the associated constraints in $\mathcal{U}_0$, defines the necessary defocus so that the thermal power induced by solar radiation does not degrade the HTF. Finally, the fourth term defines the switching between start-up and nominal operating modes.

3.4.1.1 Analytical solution analysis

Given the objective function of the problem P_0, the Hamiltonian is

$$\begin{aligned}\mathcal{H}_0 = c_0\,(T_{c,ref} - T_c)^2 + c_1\,m_c^2 - \alpha_{op}\,\gamma\,G\,I + \beta\,(T_{c,rec} - T_c) \\ + \lambda_1\left(a_1\,\gamma\,I - a_2\,m_c\,(T_c - T_{tf}) - a_3\,\tilde{H}_l\,(T_m, T_{amb})\right),\end{aligned} \tag{29}$$

and the Lagrangian with constraints directly adjoined is

$$\begin{aligned}\mathcal{L}_0 = \mathcal{H}_0 - \mu_1\,\alpha_{op}\,\gamma\,G\,I + \mu_2\,G\,(\alpha_{op}\,\gamma\,I - \alpha_{op,max}\,I_{max}) \\ + \mu_3\,(m_{c,min} - m_c) + \mu_4\,(m_c - m_{c,max}) - \mu_5\,\beta + \mu_6\,(\beta - 1),\end{aligned}$$

where

$$\begin{aligned}\dot{\lambda}_1^{opt} = 2\,c_0\,(T_{c,ref} - T_c) + \beta \\ - \lambda_1\left(\gamma\,I\frac{\partial a_1}{\partial T_c} - \frac{\partial a_2}{\partial T_c}m_c\,(T_c - T_{tf}) - a_2\,m_c - \frac{\partial a_3}{\partial T_c}\tilde{H}_l - a_3\frac{\partial \tilde{H}_l}{\partial T_c}\right),\end{aligned} \tag{30}$$

$$\lambda_1^{opt}(t_f) = 0, \tag{31}$$

$\mu_i \in \mathbb{R}$, for $i \in \{1, \ldots, 6\}$, are the Lagrange multipliers with

$$\begin{aligned}\mu_1 \geq 0, &\quad \mu_1\,\alpha_{op}\,\gamma\,G\,I = 0, \\ \mu_2 \geq 0, &\quad \mu_2\,G\,(\alpha_{op}\,\gamma\,I - \alpha_{op,max}\,I_{max}) = 0, \\ \mu_3 \geq 0, &\quad \mu_3\,(m_{c,min} - m_c) = 0, \\ \mu_4 \geq 0, &\quad \mu_4\,(m_c - m_{c,max}) = 0, \\ \mu_5 \geq 0, &\quad \mu_5\,\beta = 0, \\ \mu_6 \geq 0, &\quad \mu_6\,(\beta - 1) = 0,\end{aligned} \tag{32}$$

and

$$a_1 = \frac{\alpha_{op}\,G}{\rho_c\,c_{p,c}\,A_e}, \qquad a_2 = \frac{1}{\rho_c\,A_e\,\eta\,S_{loop}}, \qquad a_3 = \frac{1}{\rho_c\,c_{p,c}\,A_e\,S_c}.$$

The local minimum condition for the Lagrangian is

$$\frac{\partial \mathcal{L}_0}{\partial \gamma} = I\left(a_1\,\lambda_1 - \alpha_{op}\,G\right) + \alpha_{op}\,G\,I\,(\mu_2 - \mu_1), \tag{33}$$

$$\frac{\partial \mathcal{L}_0}{\partial m_c} = 2\,c_1\,m_c - \lambda_1\,a_2\,(T_c - T_{tf}) + \mu_4 - \mu_3, \tag{34}$$

$$\frac{\partial \mathcal{L}_0}{\partial \beta} = T_{c,rec} - T_c + \mu_6 - \mu_5. \tag{35}$$

A complete solution to this problem requires that the restricted and unrestricted arcs of an optimal trajectory be joined to satisfy the conditions (32)-(35). Although there are many different cases that can occur, the nature of the ideal solution precludes the possibility of multiple cases. In the following, it is analyzed the conditions on when and where the switching of the control variables can occur.

First, consider $t \in [0, t_N]$. Then, using (5) and Assumption 3, it follows that (4) can be rewritten to

$$\frac{dT_c}{dt} = -\frac{m_c\,(T_c - T_{tf})}{\rho_c\,A_e\,\eta\,S_{loop}} - \frac{\tilde{H}_l\,(T_m, T_{amb})}{\rho_c\,c_{p,c}\,A_e\,S_c} < 0.$$

Let $T_c(0) = T_c^0$, with $T_c^0 \in \mathbb{R}$ such that $T_c^0 < T_{c,rec}$ (see Assumption 2). Then, $T_{c,rec} - T_c > 0\ \forall t \in [0, t_N]$, and therefore, by the minimum principle of Pontryagin and (35), it follows that $\beta = 0$, $\forall t \in [0,\, t_N]$. Similarly, switching from $\beta = 0$ to $\beta = 1$ in the time interval $[t_D,\, t_f]$ is not possible since $\frac{dT_c}{dt} < 0$, $\forall t \in [t_D,\, t_f]$.

Since $T_c < T_{c,rec}\ \forall t \in [0, t_N]$, it follows that there exists $\bar{t} \in (t_N,\, t_f]$ such that $T_c \leq T_{c,rec}\ \forall (t_N,\, \bar{t}]$. This is expected in the early hours of the day, as the available solar radiation is low in that time interval. If $\bar{t} < t_D$, then $T_c - T_{c,rec} > 0\ \forall t \in (\bar{t},\, \underline{t})$, where $\underline{t} < t_f$. Therefore, since $T_c - T_{c,rec} > 0\ \forall t \in (\bar{t},\, \underline{t}$ and due to the minimum principle of Pontryagin, β switches from 0 to 1 at $\bar{t}$ and remains there $\forall t \in [\bar{t},\, \underline{t}]$. Finally, it must be noted that a switching of β from 0 to 1 at the time interval $[t_D,\, t_f]$ cannot happen because $\frac{dT_c}{dt} < 0$ in that time interval.

The behavior of β is natural: dispatching HTF to the hot TES system during the night would not be useful, since the solar collector field only experiences heat losses in that time period.

Now, consider the time interval $t \in [\bar{t}_{\gamma_1},\, \bar{t}_{\gamma_2}]$, with $0 < \bar{t}_{\gamma_1} < \bar{t}_{\gamma_2} < t_f$ such that the inequalities

$$0 \leq \alpha_{op}\,\gamma\,G\,I \leq \alpha_{op,max}\,G\,I_{max},$$

are not active. Note that this only can happen during the day time because $\alpha_{op}\,\gamma\,G\,I = 0\ \forall t \in [0,\, t_N] \bigcup [t_D, t_f]$. Additionally, $\gamma = 1\ \forall t \in [\bar{t}_{\gamma_1},\, \bar{t}_{\gamma_2}]$, since any other value of γ lower than 1 will result in a worse payoff. In other words, the control system will always seek to maintain the collectors fully focused when the heat induced by solar radiation does not exceed the maximum allowed value. For the time interval where the constraint $\alpha_{op}\,\gamma\,G\,I \leq \alpha_{op,max}\,G\,I_{max}$ is active, it follows that $\gamma = \frac{\alpha_{op,max}\,I_{max}}{\alpha_{op}\,I}$ minimizes the functional in (28). Note that this last equality is valid since I and α_{op} are strictly greater than zero when this constraint is active.

Turning the attention to m_c, it can be seen that $m_c(t) = m_c^{max}\ \forall t \in [0,\, t_N] \bigcup [t_D, t_f]$ will result in the minimum payoff in the cost function (28) because in this case the heat losses by convection in the solar collector field are lower than any other value of m_c in the interval $[m_{c,min}, m_{c,max})$.

During the day period, and when $c_1 > 0$ and the m_c constraints are inactive, (34) reduces to $2\,c_1\,m_c - \lambda_1\,a_2\,(T_c - T_{tf}) = 0$, which it leads to

$$m_c = \lambda_1 \frac{a_2\,(T_c - T_{tf})}{2\,c_1}. \tag{36}$$

Furthermore, as $\frac{\partial^2 \mathcal{H}_0}{\partial m_c^2} = 2\,c_1 > 0$, the above control law actually minimizes (globally) the Hamiltonian. However, since (36) depends on the solution of the boundary value problem (30)-(31), which is nonlinear, it is hard to define an analytic and explicit control policy, and consequently, a numerical solution must be considered. More details on this will be given in Sections 3.5 and Chapter 5.

For the special case in which $c_1 = 0$, the optimal trajectory of m_c during the day period can be computed in the following manner. If $T_c < T_{c,ref}$, then $m_c = m_c^{min}$ must be applied into the system in order to obtain the maximum temperature increment of the HTF in the solar field and the minimum payoff in the cost function (28). When $T_c = T_{c,ref}$, then

$$m_c = \frac{\eta\,S_{loop}}{c_{p,c}\,(T_c - T_{tf})}\left(\alpha_{op}\,\gamma\,G\,I - \frac{\tilde{H}_l\,(T_m, T_{amb})}{S_c}\right),$$

must be applied into the system, since this guarantees that $\frac{dT_c}{dt} = 0$, and consequently, the payoff of the first term of the functional in (28) will be null in this time interval. Similarly, if $T_c > T_{c,ref}$, then $m_c = m_c^{max}$ must be applied into the system in order to get the maximum decrease in the outlet temperature variation.

It is important to emphasize that most of the above analysis is qualitative and it is important to get an insight into what must be expected when (28) is solved. For its solution, however, it is advisable to use direct methods because of the technical difficulty in solving the costate and state differential equations together with the constraints.

3.4.2 Thermal Energy Storage

As already described in Section 2.3, the dispatch of the hot TES system to the power block aims to maximize the daily revenue from the electricity sales by manipulating the outlet mass flow rate of the hot TES system. Additionally, this control system must avoid the power block operation below a minimum load, its repeated re-starts during the same day as well as fast changes and oscillations of the mass flow rate. These constraints are technically challenging to be treated in OCPs, because they involve control derivatives in the cost function. To tackle this issue, in this work the outlet mass flow rate of the hot TES system will be split into two auxiliary control variables together with additional constraints in order to reduce the control problem into an ordinary one. More precisely, let $m_p = m_p^a + m_p^d$, with m_p^a absolute continuous and m_p^d a step function, such that $m_p^d \leq 0$. Then, $\frac{dm_p}{dt} = \frac{dm_p^a}{dt}$ and defining $r = \frac{dm_p}{dt}$, it follows that $\frac{dm_p^a}{dt} = r$, i. e.,

r determines the absolute continuous part of m_p. In other words, the problem of finding m_p is rewritten as the problem of finding r and m_p^d.

Now, let $U_1 = (r,\, m_p^d,\, Q)$. Then, the following optimization problem is formulated for the time interval $t \in [0, t_f]$:

$$
\begin{aligned}
P_1: \quad & \min_{U_1(t)\in\mathcal{U}_1} \int_0^{t_f} \Big(-\alpha_p\,(m_p^a + m_p^d)\,P_w \\
& \qquad + c_2\,(T_{tf,ref} - T_{tf})^2 + c_3\,m_p^d\,(m_p^{mop} - m_p^a) \\
& \qquad\qquad + c_4\,r^2 + c_5\,Q^2\Big)\,dt, \\
\text{s. t.:} \quad & \\
& L_{tq}\,A_{tq}\left(h_{tq}\frac{d\rho_{tq}}{dT_{tq}} + \rho_{tq}\frac{dh_{tq}}{dT_{tq}}\right)\frac{dT_{tq}}{dt} = \\
& \qquad m_c\,\beta\,(h_{T_c} - h_{tq}) - \tilde{P}_l\,(T_{tq} - T_{amb}), \\
& L_{tf}\,A_{tf}\left(h_{tf}\frac{d\rho_{tf}}{dT_{tf}} + \rho_{tf}\frac{dh_{tf}}{dT_{tf}}\right)\frac{dT_{tf}}{dt} = \\
& \qquad m_c\,(1-\beta)\,(h_{T_c} - h_{tf}) + m_p\,(h_p - h_{tf}) \\
& \qquad\qquad - \tilde{P}_l\,(T_{tf} - T_{amb}) + Q, \\
& A_{tq}\,\rho_{tq}\frac{dL_{tq}}{dt} = m_c\,\beta - (m_p^a + m_p^d), \\
& A_{tf}\,\rho_{tf}\frac{dL_{tf}}{dt} = m_p - m_c\,\beta, \\
& \frac{dm_p^a}{dt} = r, \\
& 0 \le L_{tq} \le L_{tq,max}, \\
& 0 \le L_{tf} \le L_{tf,max}, \\
& T_{tq}(0) = T_{tq}^0, \qquad T_{tf}(0) = T_{tf}^0, \\
& L_{tq}(0) = 0, \qquad L_{tf}(0) = L_{tf}^0, \\
& m_p^a(0) = 0,
\end{aligned}
\tag{37}
$$

with

$$
\mathcal{U}_1 \;=\; \{(r,\, m_p^d,\, Q) \;\in\; \mathbb{R}^3 \;\mid\; 0 \;\le\; Q \;\le\; Q_{max},\, m_p^d \;\le\; 0,\; 0 \;\le\; m_p^a + m_p^d \;\le\; m_p^{max}\}.
$$

In (37), the efficiency of the power block is given by α_p, while $c_2,\, c_3 > 0$ and $c_4,\, c_5 \ge 0$. Note that the first term of the functional in (37) is responsible for the instant revenue from the sale of electricity. The price of the electricity produced is given by $P_w = TOD \cdot PPA$, in which TOD is the time of day and PPA (*Power Purchase Agreement*) represents the energy purchase [Price/kW]. The second term of the functional in (37) has been included to keep the fluid temperature in the cold storage tank at the desired reference value $T_{tf,ref}$. In turn, the third term prevents the power block from working below the minimum operating mass flow rate, m_p^{mop}, with $m_p^{mop} \in (0,\, m_p^{max})$, and the fourth term was introduced to penalize rapid changes in r. The fifth term of the functional in (37) penalizes rapid changes in the heat induced by the electrical resistance in the cold fluid storage tank. Finally, the last two inequalities in (37) were included to restrict the liquid levels in the storage tanks within the feasible range of operation.

3.4.2.1 Analysis of the analytical solution of the simplified linearized problem

In this section, P_1 is simplified to a linear OCP with simple dynamics in order to derive the analytical solution. This allows to characterize how the optimal solution evolves along the day in a qualitative way. Here, the specific mass and enthalpy in the equations (8)-(15) are considered constant, i.e., $\rho_i = \overline{\rho}_i$ and $h_j = \overline{h}_j$, for $i \in \{tq,\, tf\}$ and $j \in \{T_c,\, p,\, tq,\, tf\}$. Additionally, the terms L_{tq} and L_{tf} in the left-hand side of (14)-(15) are simplified to positive constants. Thus, $L_{tq} = \overline{L}_{tq}$ and $L_{tf} = \overline{L}_{tf}$ in the left-hand side of (14)-(15).

In this case, the Hamiltonian of the simplified problem P_1 is

$$\begin{aligned}\mathcal{H}_1 = &-\alpha_p\,(m_p^a + m_p^d)\,P_w + c_2\,\left(T_{tf,ref} - T_{tf}\right)^2 + c_3\,m_p^d\,(m_p^{mop} - m_p^a) + c_4\,r^2 + c_5\,Q^2 \\ &+ \lambda_2\,a_4\Big(m_c\,(1-\beta)\,(\overline{h}_{T_c} - \overline{h}_{tf}) + m_p\,(\overline{h}_p - \overline{h}_{tf}) - \tilde{P}_l\,(T_{tf} - T_{amb}) + Q\Big) \\ &+ \lambda_3\,a_5\left(m_c\,\beta - (m_p^a + m_p^d)\right) + \lambda_4\,a_6\,(m_p - m_c\,\beta) + \lambda_5\,r,\end{aligned}$$

where

$$\begin{aligned}a_4 &= \left(\overline{L}_{tf}\,A_{tf}\left(\overline{h}_{tf}\frac{d\rho_{tf}}{dT_{tf}} + \overline{\rho}_{tf}\frac{dh_{tf}}{dT_{tf}}\right)\right)^{-1}, \\ a_5 &= \frac{1}{A_{tq}\,\overline{\rho}_{tq}}, \\ a_6 &= \frac{1}{A_{tf}\,\overline{\rho}_{tf}}.\end{aligned}$$

The Lagrangian is

$$\begin{aligned}\mathcal{L}_1 = \mathcal{H}_1 &- \nu_1\,L_{tq} + \nu_2\,(L_{tq} - L_{tq,max}) - \nu_3\,L_{tf} + \nu_4\,(L_{tf} - L_{tf,max}) \\ &- \vartheta_1\,Q + \vartheta_2\,(Q - Q_{max}) - \vartheta_3 m_p^d - \vartheta_4\,(m_p^a + m_p^d) + \vartheta_5\,(m_p^a + m_p^d - m_p^{max}),\end{aligned}$$

where $\nu_i \in \mathbb{R}$, for $i \in \{1, \ldots, 4\}$, and $\vartheta_j \in \mathbb{R}$, for $j \in \{1, \ldots, 5\}$, are the Lagrange multipliers with

$$\begin{aligned}&\nu_1 \geq 0, && \nu_1\,L_{tq} = 0, \\ &\nu_2 \geq 0, && \nu_2\,(L_{tq} - L_{tq,max}) = 0, \\ &\nu_3 \geq 0, && \nu_3\,L_{tf} = 0, \\ &\nu_4 \geq 0, && \nu_4\,(L_{tf} - L_{tf,max}) = 0,\end{aligned}$$

and

$$\begin{aligned}
\vartheta_1 &\geq 0, & \vartheta_1\, Q &= 0,\\
\vartheta_2 &\geq 0, & \vartheta_2\, (Q - Q_{max}) &= 0,\\
\vartheta_3 &\geq 0, & \vartheta_3\, m_p^d &= 0,\\
\vartheta_4 &\geq 0, & \vartheta_4\, (m_p^a + m_p^d) &= 0,\\
\vartheta_5 &\geq 0, & \vartheta_5\, (m_p^a + m_p^d - m_p^{max}) &= 0.
\end{aligned}$$

Set $c_2,\, c_3 > 0$, and $c_4,\, c_5 \geq 0$, and let T_{tf}^{opt}, T_{tq}^{opt}, L_{tq}^{opt}, L_{tf}^{opt}, and $m_p^{c,\,opt}$ be the optimal trajectories of the control problem P_1. Then,

$$\begin{aligned}
\dot{\lambda}_2^{opt} &= 2\, c_2\, (T_{tf,ref} - T_{tf}) - \lambda_2\, a_4\, \tilde{P}_l,\\
\dot{\lambda}_3^{opt} &= \nu_2 - \nu_1,\\
\dot{\lambda}_4^{opt} &= \nu_4 - \nu_3,\\
\dot{\lambda}_5^{opt} &= -\alpha_p\, P_w + c_3\, m_p^d - \lambda_3\, a_5 + \lambda_4\, a_6 \frac{\partial m_p}{\partial m_p^a} + \vartheta_5 - \vartheta_4,
\end{aligned}$$

with boundary conditions

$$\lambda_i^{opt}(t_f) = 0,\ i \in \{2,\, \ldots,\, 5\}.$$

The local minimum condition for the Lagrangian is

$$\begin{aligned}
\frac{\partial \mathcal{L}_1}{\partial r} &= 2\, c_4\, r + \lambda_5,\\
\frac{\partial \mathcal{L}_1}{\partial m_p^d} &= -\alpha_p\, P_w + c_3\, (m_p^{mop} - m_p^c) + \vartheta_5 - \vartheta_4 - \vartheta_3,\\
\frac{\partial \mathcal{L}_1}{\partial Q} &= 2\, c_5\, Q + a_4\, \lambda_2 + \vartheta_2 - \vartheta_1.
\end{aligned}$$

Now, an analysis of the linearized OCP P_1 can be performed as follows. From the previous subsection, $\beta(t) = 0\ \forall t \in [0, t_N]$. Then, since $L_{tq}(0) = 0$, it follows that $m_p(t) = 0\ \forall t \in [0, t_N]$, because in this time interval there will be no energy in the hot TES system to be dispatched to the power block, i.e., $L_{tq}(t) = 0\ \forall t \in [0, t_N]$. Thus, $m_p^d = m_p^a = r = 0$ in this time interval.

Let $\underline{t}$ and $\bar{t}$ be positive constants such that $t_N < \underline{t} < \bar{t} < t_f$ and $\forall t \in [\underline{t},\, \bar{t}]$ the inequality $T_c(t) > T_{c,rec}$ holds. Then, $\beta(t) = 1\ \forall t \in [\underline{t},\, \bar{t}]$ and if $m_p(t) = 0\ \forall t \in [\underline{t},\, \bar{t}]$, it follows that $L_{tq}(t) > 0$ in that time interval.In this case, it would be possible to dispatch the HTF in the hot TES system to the power block. Note that at least one switch from $m_p = 0$ to $m_p = \overline{m}_p$, with $\overline{m}_p \in (0,\, m_p^{max}]$, needs to occur at $t \in [\underline{t},\, t_f)$; otherwise, $m_p(t) = 0$ at all times results in

$$\int_0^{t_f} \alpha_p\, \underbrace{(m_p^a + m_p^d)}_{m_p}\, P_w\, dt = 0.$$

Since $\alpha_p\,(m_p^a + m_p^d)\,P_w$ is non-negative by construction, a switch of m_p from 0 to $\overline{m}_p$ can do no worse than that (see the functional in (37)). If $m_p^a < m_p^{mop}$, it follows that $(m_p^{mop} - m_p^a) > 0$, and consequently, the payoff $c_3\,m_p^d\,(m_p^{mop} - m_p^a)$ is minimum if $m_p^d = -m_p^a$. Therefore, $m_p = m_p^a + m_p^d = 0$ if $m_p^a < m_p^{mop}$. Similarly, if $m_p^a > m_p^{mop}$, then $(m_p^{mop} - m_p^a) < 0$ and the payoff $c_3\,m_p^d\,(m_p^{mop} - m_p^a)$ is minimized for $m_p^d = 0$, which means that $m_p = m_p^a$.

3.5 PRACTICAL IMPLEMENTATION

The proposed optimal controller results in both implementational and computational challenges. First, it requires the forward-in-time solution to the solar field and TES systems and the backward-in-time solution to the adjoint equations. Additionally, the state control variables of the two optimal controllers are coupled. In particular, the mass flow rate and outlet temperature of the solar collector field are coupled with the hot TES, and similarly, the outlet temperature of the cold TES is coupled with the solar collector field as can be seen in Figure 11. A way to address these computational challenges is to implement the optimal control problem in a configuration close to model-based predictive control: the time interval $[0, t_f]$ is divided into N (for some $N \in \mathbb{N}$) shorter time intervals of length $\frac{t_f}{N}$ and the solution of the following problem:

$$
\begin{aligned}
&\min_{U_0(t)\in\mathcal{U}_0} \int_{j\frac{t_f}{N}}^{t_f} \Big(c_0\left(T_{c,ref} - T_c\right)^2 + c_1\left(m_c\right)^2 \\
&\qquad\qquad -\alpha_{op}\,\gamma\,G\,I + \beta\left(T_{c,rec} - T_c\right)\Big) dt, \\
&\text{s. t.:} \\
&\qquad \rho_c\,c_{p,c}\,A_e\,\tfrac{dT_c}{dt} = \alpha_{op}\,\gamma\,G\,I - \tfrac{c_{p,c}\,m_c\,(T_c - T_{tf})}{\eta\,S_{loop}} \\
&\qquad\qquad - \tfrac{\tilde{H}_l\,(T_m, T_{amb})}{S_c}, \\
&\text{with } T_c\left(j\tfrac{t_f}{N}\right) \text{ given}
\end{aligned}
\tag{38}
$$

is calculated, for $j \in \{0, \ldots, N-1\}$. In detail, once a control action (calculated by the present scheme) is applied to the time instant $j\frac{t_f}{N}$ in the real plant, the state variables are measured at the time $j\frac{t_f}{N}$ and the problem (38) is then solved online using a direct method. Additionally, the solar radiation and ambient temperature applied to the system along the time interval $t \in [j\frac{t_f}{N}, T]$ are considered perfectly known and equal to those applied to the real plant.

Then, the optimal states and control variables obtained from (38) are used to

solve

$$
\begin{aligned}
&\min_{U_1(t)\in\mathcal{U}_1} \int_{j\frac{t_f}{N}}^{t_f} \Big(-\alpha_p\,(m_p^a + m_p^d)\,P_w + c_2\,(T_{tf,ref} - T_{tf})^2 \\
&\qquad\qquad +c_3\,m_p^d\,\left(m_p^{mop} - m_p^a\right) + c_4 r^2 + c_5 Q^2\Big)\,dt, \\
&\text{s. t.:} \\
&L_{tq}\,A_{tq}\left(h_{tq}\frac{d\rho}{dT_{tq}} + \rho_{tq}\frac{dh}{dT_{tq}}\right)\frac{dT_{tq}}{dt} = \; m_c\,\beta\,(h_{T_c} - h_{tq}) \\
&\qquad\qquad -\tilde{P}_l\,(T_{tq} - T_{amb}), \\
&L_{tf}\,A_{tf}\left(h_{tf}\frac{d\rho}{dT_{tf}} + \rho_{tf}\frac{dh}{dT_{tf}}\right)\frac{dT_{tf}}{dt} = \\
&\qquad m_c\,(1-\beta)\,(h_{T_c} - h_{tf}) + m_p\,(h_p - h_{tf}) \\
&\qquad\qquad -\tilde{P}_l\,(T_{tf} - T_{amb}) + Q, \\
&A_{tq}\,\rho_{tq}\,\frac{dL_{tq}}{dt} = m_c\,\beta - (m_p^a + m_p^d), \\
&A_{tf}\,\rho_{tf}\,\frac{dL_{tf}}{dt} = m_p - m_c\,\beta, \\
&\frac{dm_p^a}{dt} = r, \\
&0 \le L_{tq} \le L_{tq,max}, \\
&0 \le L_{tf} \le L_{tf,max}, \\
&\text{with } T_{tq}\left(j\tfrac{t_f}{N}\right),\, T_{tf}\left(j\tfrac{t_f}{N}\right),\, L_{tq}\left(j\tfrac{t_f}{N}\right),\, L_{tf}\left(j\tfrac{t_f}{N}\right), \\
&\text{and } m_p^a\left(j\tfrac{t_f}{N}\right) \text{ given},
\end{aligned}
\tag{39}
$$

in a similar fashion as (38). The control actions $U_0(t)$ and $U_1(t)$ are then applied between $j\frac{t_f}{N}$ and $(j+1)\frac{t_f}{N}$, where the procedure is started again. Note that the solution of (38)-(39) is connected with the value of the function of the original problem, since it calculates the cost at the instant $j\frac{t_f}{N}$.

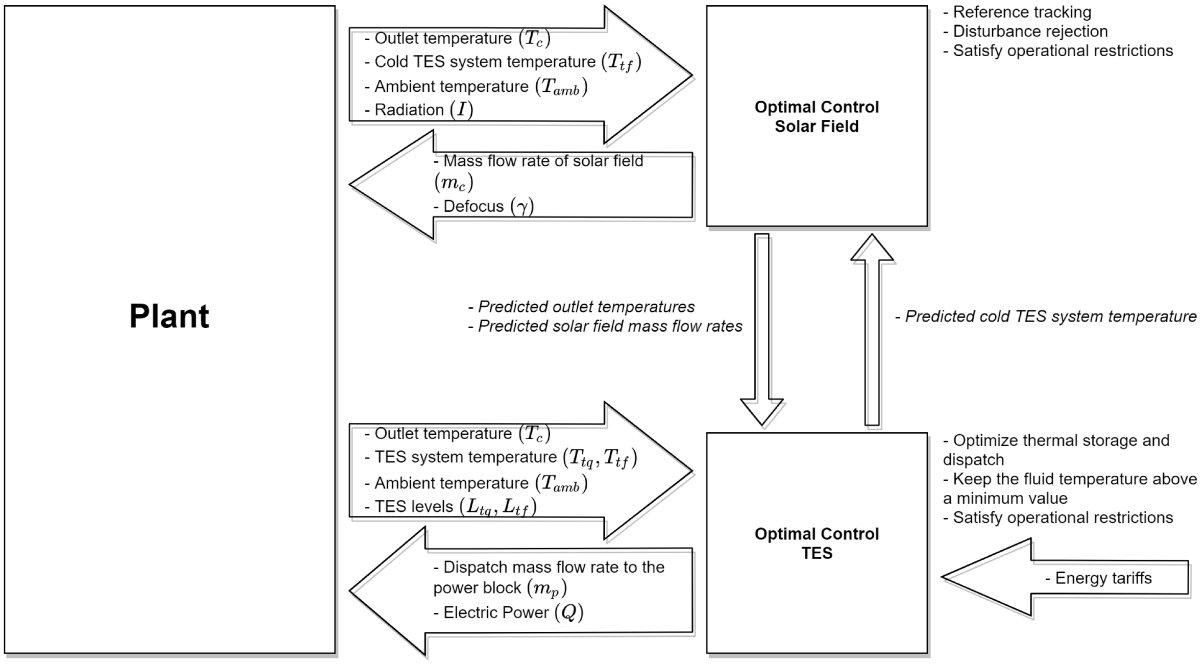

Figure 11 – Solar plant diagram.

Algorithm 1: OCP based on direct multiple shooting method

States: $X = [x_1, \ldots, x_{N+1}]$;
Controls: $U = [u_1, \ldots, u_N]$;
Parameters: $P = [P1_1, \ldots, P1_N, P2_1, \ldots, P2_N, \ldots]$; `// All the Exogenous Signals: Radiation, Ambient temperature, Optical efficiency and Coupling variables`
$g = [X_1 - InitialState]$; `// The vector that will contain all the states trajectories to be continuous`
for $k = 1 : N$ **do**
    $X_{next} := \int f(X_k, U_k)$; `// Solve RK4 method (24). The numerical solution of the IVPs for all ODEs, during the N subintervals.`
    $s_{k+1} := X_{k+1} - X_{next}$; `// Equation (25)`
    $g = [g; s_{k+1}]$;
    $J = \sum J(X_k, U_k, P_k)$; `// Equation (26)`
end
$g.lb = [0, 0, \ldots, N]$; `// Define continuity path constraints for` g
$g.up = [0, 0, \ldots, N]$; `// Define continuity path constraints for` g
$x.lb = [\underline{x_1}, \ldots, \underline{x_{N+1}}; \underline{u_1}, \ldots, \underline{u_N}]$; `// Define lower bound path constraints for states and controls`
$x.ub = [\overline{x_1}, \ldots, \overline{x_{N+1}}; \overline{u_1}, \ldots, \overline{u_N}]$; `// Define upper bound path constraints for states and controls`
$x0 = [1, \ldots, N+1]$; `// Define the initial value of the optimization variables for N+1 states`
$u0 = [1, \ldots, N]$; `// Define the initial value of the optimization variables for N controls`
for $i = 2 : end$ **do**
    $args.p = [InitialStates; Reference; P]$;
    $args.x0 = [x0; u0]$; `// Initial value of the optimization variables for N+1 states and N controls`
    solve$(J, args.x0, x.lb, x.up, g, g.lb, g.up, args.p,)$; `// Solve the NLP`
    Save the first control solutions and use them to solve the first part of ODEs. The state solution will become an $InitialState$;
    Shift the states and control solutions and set them as an initial value of the optimization variables $args.x0$ for the next iteration. The last states and controls will be repeated.;
    Shift the exogenous signals in P for the next iteration.;
end

4 CLASSIC CONTROL STRATEGIES

In this Chapter, two classic control strategies for controlling the solar plant described in Chapter 2 will be described. These approaches follow the concepts of Wagner and Gilman (2011) and aim at satisfying the nominal power cycle demand by making use of the available resources in the TES system, while ensuring that the operative constraints are satisfied. Both strategies consider a PI controller with an anti-windup methodology for the regulation of the outlet temperature of the solar collector field, where the design parameters where obtained based on the AMIGO tuning rule (ÅSTRÖM; HÄGGLUND, 2005). This tuning rule methodology is based on a first-order transfer function plus dead time of the system. A feedforward controller is also considered for defocusing the solar field when it exceeds the nominal thermal power of the plant. This control law was obtained from the steady-state solution of (4) for γ and assuming that $T_c = T_{ref}$. For temperature control of the cold TES, a simple on/off control police is used. The difference between the approaches lies in the way of calculating the dispatch/storage of the HTF in the hot TES and will be described in the next sections.

4.1 STATIC DISPATCH SYSTEM

In this case, the dispatch of the hot TES system is determined by logical statements which depend on the level of the hot TES system (adjusted monthly based on future availability of solar radiation) and the information about the energy tariff prices. A schematic diagram of methodology is shown in Figure 12. Importantly, the sampling time considered for this approach is equal to 30 s and on each iteration, the algorithm verifies if the level of the hot TES system is above a pre-specified value and if the current time is a priority time, which is associated with the mean maximum value of the expected energy tariff price. When either of these conditions is true the HTF in the hot TES system is dispatched to the power block considering the maximum mass flow rate. In other words, this strategy finds the switching time instants that the control variable m_p switches from one extreme to the other.

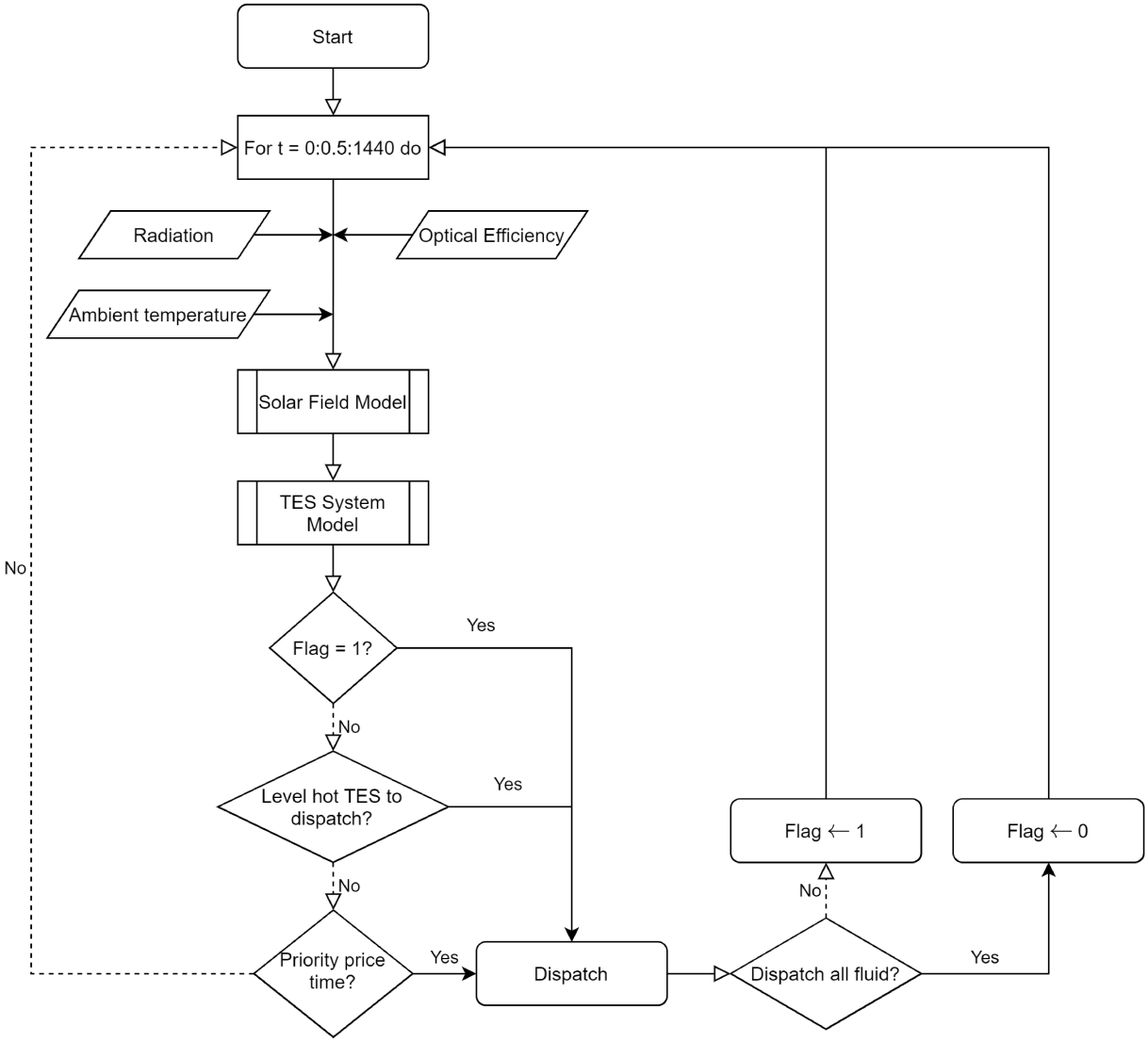

Figure 12 – Diagram of the Static Dispatch System.

4.2 DYNAMIC DISPATCH SYSTEM

This second control strategy improves the system revenue using a priority dispatch list, which contains the time instant of the day where the system must dispatch the HTF to power block on each day. The computation of these time instants are performed as follows. First, the solar collector field subsystem is simulated decoupled from the TES system[1] in order to define its outlet mass flow rate and temperature behavior during the day. These data are then used in the hot TES subsystem equations to predict its behavior. With a sampling time of 30 minutes, the switching time of m_p from its minimum value to maximum value (and vice versa) is determined within the TES physical constraints. Obviously, days with a high solar radiation profile will induce high mass flow rates in the solar collector field, and consequently, the algorithm should prioritize

[1] This situation is reasonable, since the temperature of the cold TES system is approximately constant and there is always enough HTF to be directed to the solar field under normal operating conditions.

the saturation limits of the thermal energy in the TES over the energy tariff prices. For days with low solar radiation profile, thermal energy saturation is not expected and the dispatch can give priority to the maximum energy tariff price periods. A diagram of the Dynamic Dispatch System can be seen in Figure 13.

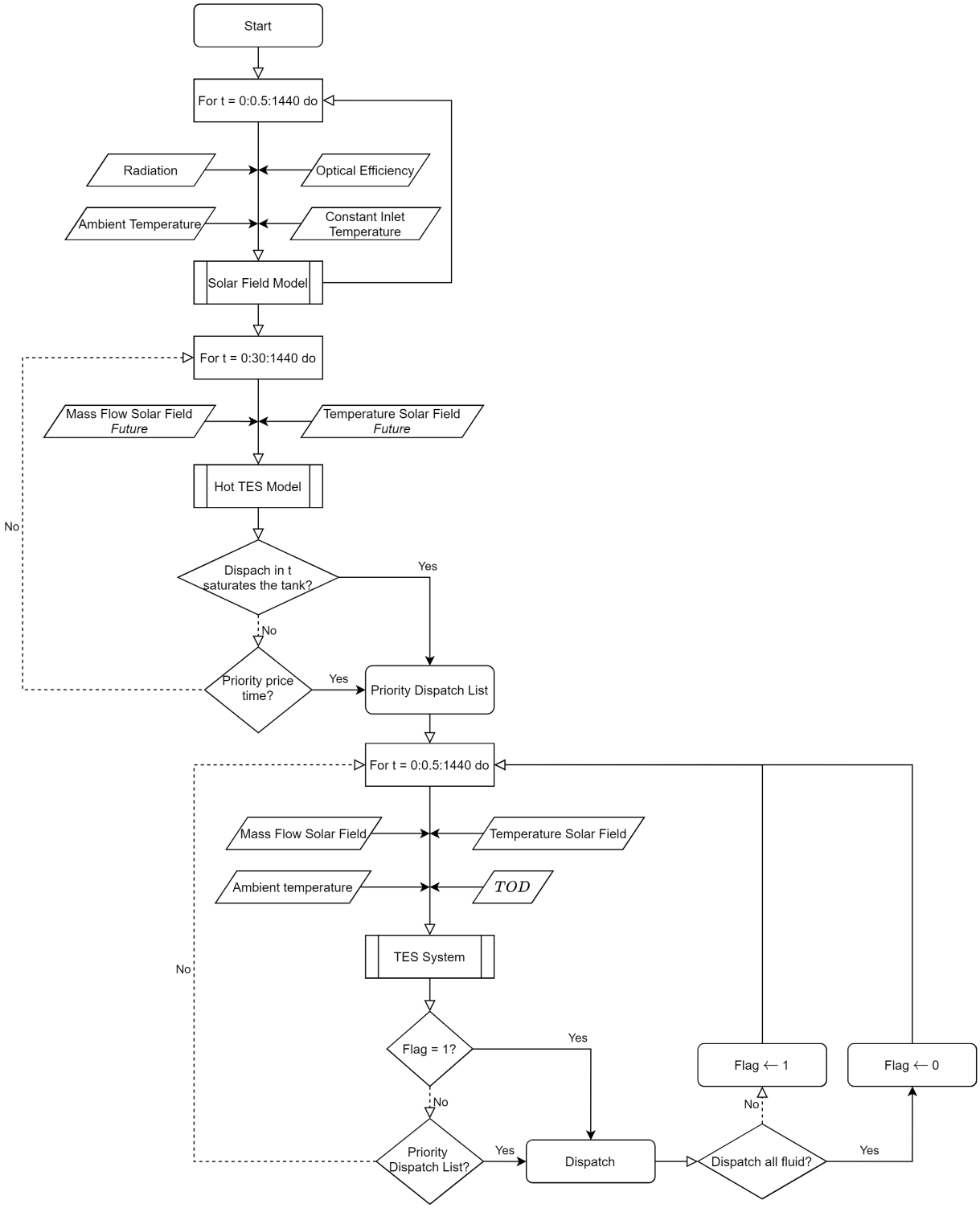

Figure 13 – Diagram of the Dynamic Dispatch System.

5 RESULTS AND DISCUSSION

In this chapter, the simulation results obtained with the Optimal Control Strategy proposed for the Brazilian and Spanish variable energy tariff prices and realistic weather data will be presented. Furthermore, a comparative study with two classic control strategies (see Chapter 4) are evaluated in order to illustrate the improvements in the revenue of the produced energy in these scenarios.

5.1 SIMULATION RESULTS FOR THE BRAZILIAN ENERGY TARIFF PRICE

The numerical tests were conducted considering (4)-(15) as a virtual plant and real data of solar radiation and ambient temperature corresponding to the Brazilian geographic location 22º41'22,65"S 45º00'22,28"W, which were obtained from the SONDA Project (INPE, 2019). The optical efficiency is generated as described in Section 2.2.2.1-2.2.2.2 and using the same geographic location. The simulations were coded in MATLAB and the CasADi package was used to solve the OCP numerically. To ensure proper numerical conditioning of the solver, the system variables were made dimensionless in order to get a system with normalized variables of similar sizes. More precisely, the outlet temperatures of the solar collector field and of the TES systems were scaled with respect to $T_{c,ref}$, the mass flow rates scaled with respect to m_p^{max}, the heat induced by the electrical heater in the cold TES system with respect to Q^{max}, and the hot and cold TES systems with respect to L_{tq}^{max} and L_{tf}^{max}, respectively. Note that in this framework the developed control methodology is still applicable without loss of generality. Importantly, the plant's solar multiple has a value of approximately 2.3 and the tanks have a storage capacity of 4 hours. The power block efficiency is $\alpha_p = 60\%$ and the (dimensionless) minimum operating mass flow rate of the power block is $m_p^{mop} = 0.54$. These values are generally considered for 3 MW_e Fresnel CSP plants (MEHOS et al., 2020).

Best practices in the control of solar plants provided by the National Renewable Energy Laboratory (NREL) indicated that, during the night, the maximum mass flow in the field of solar collectors must be lower than during the day to reduce the parasitic electrical consumption of the system (MEHOS et al., 2020). For this reason, in this work it will be considered that the maximum mass flow in the field of solar collectors is 42% lower during the night compared to the day.

The vales of the TOD were borrowed from the energy distribution company ENEL, Rio de Janeiro – Brazil. Basically, the TOD profile is constant by parts and assumes three different values along the day, namely the off-peak white tariff (0.550), intermediate white tariff (0.831) and peak white tariff (1.280), respectively. In particular, from 4:00 PM to 6:00 PM and from 9:00 PM to 10:00 PM, the TOD profile assumes the intermediate white tariff, whereas the peak white tariff covers the time interval 6:00 PM

to 9:00 PM. For the rest of the day, the TOD profile assumes the off-peak white tariff. These values came into force on 03/15/2020 under the resolution 2666/2020, as can be seen in ANEEL (2020).

In the next subsections, the performance of the optimal controller will be analyzed and a comparative study with the strategies described in Chapter 4 will be presented together with the revenue obtained.

5.1.1 Optimal Control

5.1.1.1 Solar Collector Field

Figure 14 shows the time evolution of the main variables of the solar collector field with the Optimal Control Strategy. This numerical scenario considers the plant operating over six days[1] with radiation profiles of clean and cloud days in order to impose a wide range of operating conditions and optical efficiency values (see the second graphic of Figure 14). As can be seen in the first graphic of Figure 14, the optimal controller was able to track the outlet temperature reference along the daytime in spite of the solar radiation disturbances. Interestingly, during the daytime of the first four days the controller was able to maintain the outlet temperature tracking with full reflection of the mirrors (see the third graphic of Figure 14). However, the defocusing was necessary in the last two days because of the high radiation profiles and constraints on the mass flow rate in the solar field. Note that during the night there is no outlet temperature reference tracking since the radiation is null in that time interval and the plant experiences only heat losses.

The operation modes of the plant along the simulation are shown in the bottom graphic of Figure 14. For readability reasons, the operation modes have been labeled as follows in Figure 14: 0 - night; 1 - start-up; 2 - nominal; and 3 - shut-down. In general, the start-up operation mode last between 90 to 150 minutes depending on the radiation conditions and starts when the radiation is greater than zero. As shown in Section 2.1.1, in this operation mode the HTF recirculates between the solar collector field and the cold TES until the outlet temperature of the solar collector field reaches the value specified by T_{rec}. To the point that the T_c becomes higher than T_{rec}, the valve located at the end of the solar collector field switches and the HTF is directed to the hot TES, which indicates the nominal operation mode. During the shut-down operation mode the valve switches again and the HTF recirculates between the solar collector field and the cold TES again. This behavior also happens during the night operation mode, however in the latter the hot TES is completely empty. Remarkably, in the fourth day the control system switches from nominal to the night operation mode and then switches to the

[1] Two days with normal radiation in April, two days with low radiation in June, and two days with good radiation in December, the reason why the optical efficiency and radiation intensity changes during these days.

shut-down operation mode (see the bottom graphic of Figure 14). The reason why this happens is because of the low radiation and TOD profiles, as it will be shown in the next section.

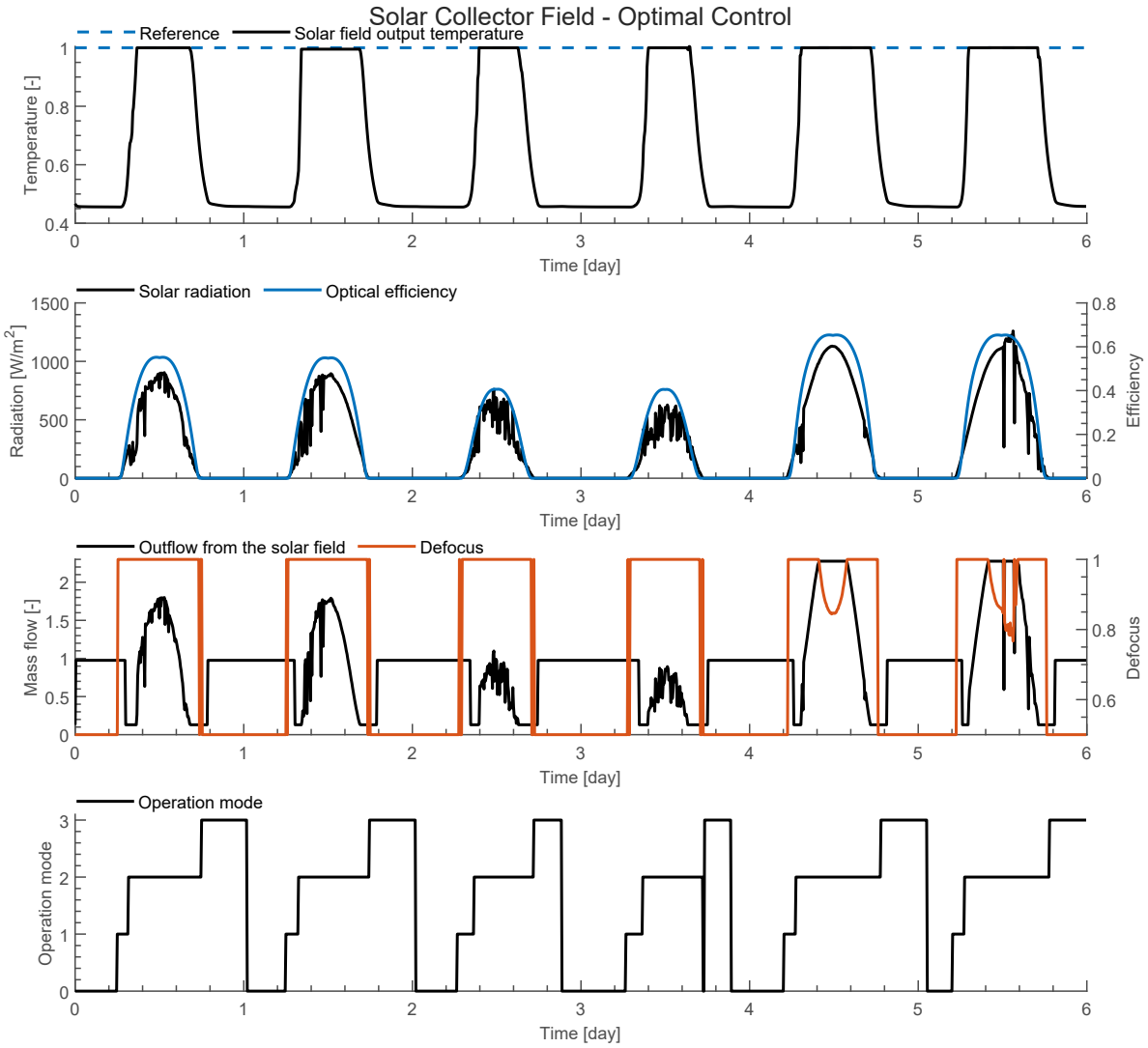

Figure 14 – Simulation results of the plant with the Optimal Control Strategy. From top to bottom, the graphics show: the outlet temperature of the field, solar irradiation and optical efficiency, defocus, mass flow rate in the solar field and operation modes.

5.1.1.2 Thermal Energy Storage

The time evolution of the variables associated with the TES are presented in Figure 15. The level and temperature of the hot and cold TES are shown in the first and second graphics of Figure 15, respectively. Note that their level remains constant along the night operation mode and the heat induced by the electrical resistance in the cold TES (bottom graphic of Figure 15) adjust its temperature to keep it close to the desired reference value. Interestingly, the electrical resistance is used almost all day

for days with low radiation profile (see the time interval between days 3 and 4 in the bottom graphic of Figure 15).

The optimal controller always dispatches the fluid in the hot TES system to the power block during the time interval with better tariff prices in order to obtain the best payoff, as can be seen in the third graphic of Figure 15. This is the reason why the dispatch starts only after the night operation mode kicks-in on the fourth day: if the outlet mass flow rate profile of the hot TES system was different in those days, then the tank could be empty during the peak white tariff and the revenue would be lower. Finally, note that the controller respects the minimum operating mass flow rate limits to the power, defined by m_p^{mop}, at the same time that it does not present repeated restarts during the same day when the dispatch starts.

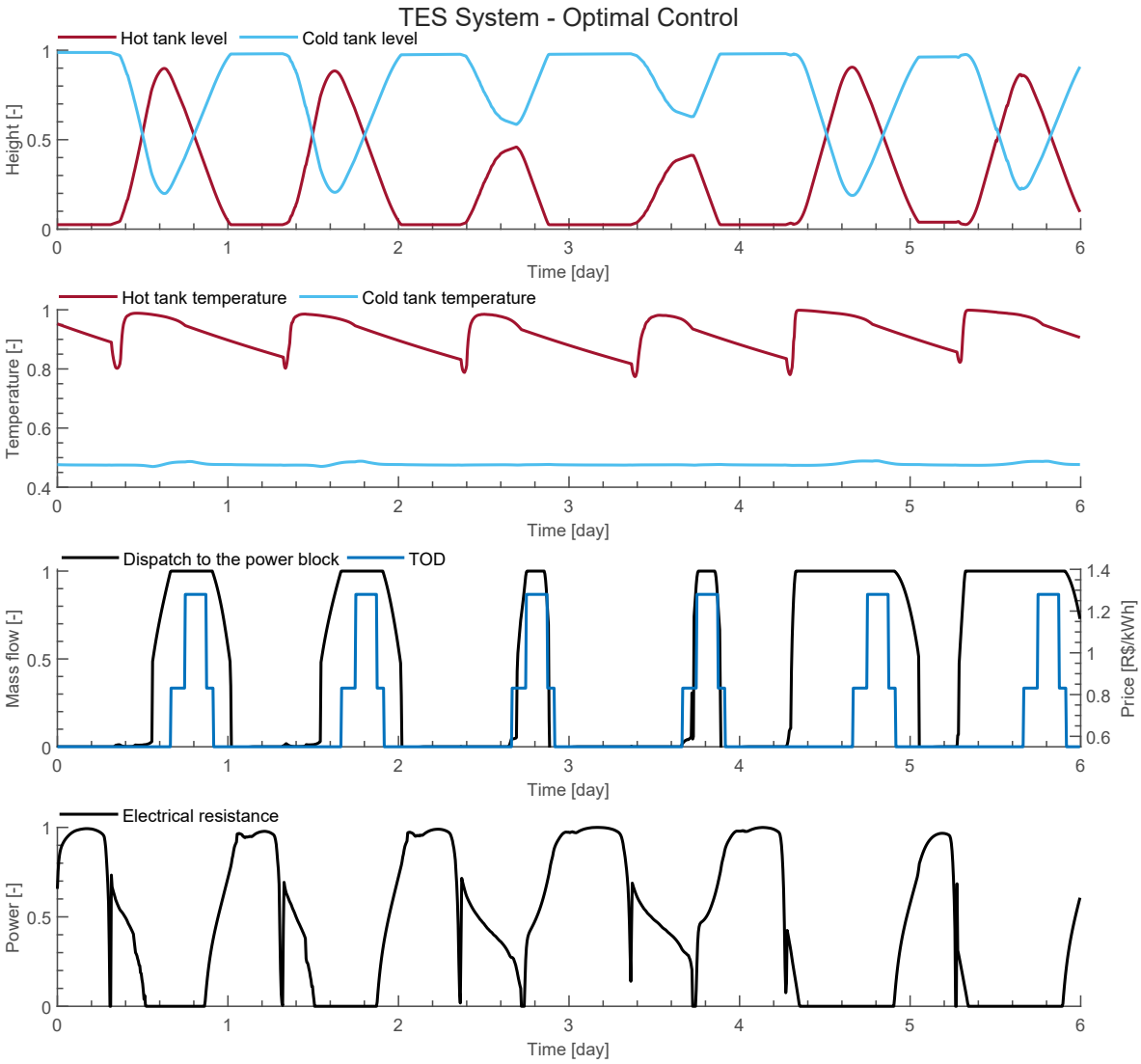

Figure 15 – Simulation results of the plant with the Optimal Control Strategy. From top to bottom, the graphics show: liquid levels in the storage tanks, HTF temperature in the storage tanks, dispatch mass flow and TOD, and electrical power induced by the resistance in the cold TES.

5.1.2 Classic Control Strategy - Static Dispatch System

5.1.2.1 Solar Collector Field

Figure 16 presents the time evolution of the main variables of the solar collector field within the Classic Control Strategy using the Static Dispatch System. This numerical simulation considers the same days and conditions as applied in the optimal control. The Classic Control Strategy was able to track the outlet temperature reference along the daytime, as can be seen in the first graphic of Figure 16. The defocusing is still necessary for the last two days when the mass flow rate in the solar field reaches the maximum value. At this point, the feedforward controller is triggered to handle the defocus.

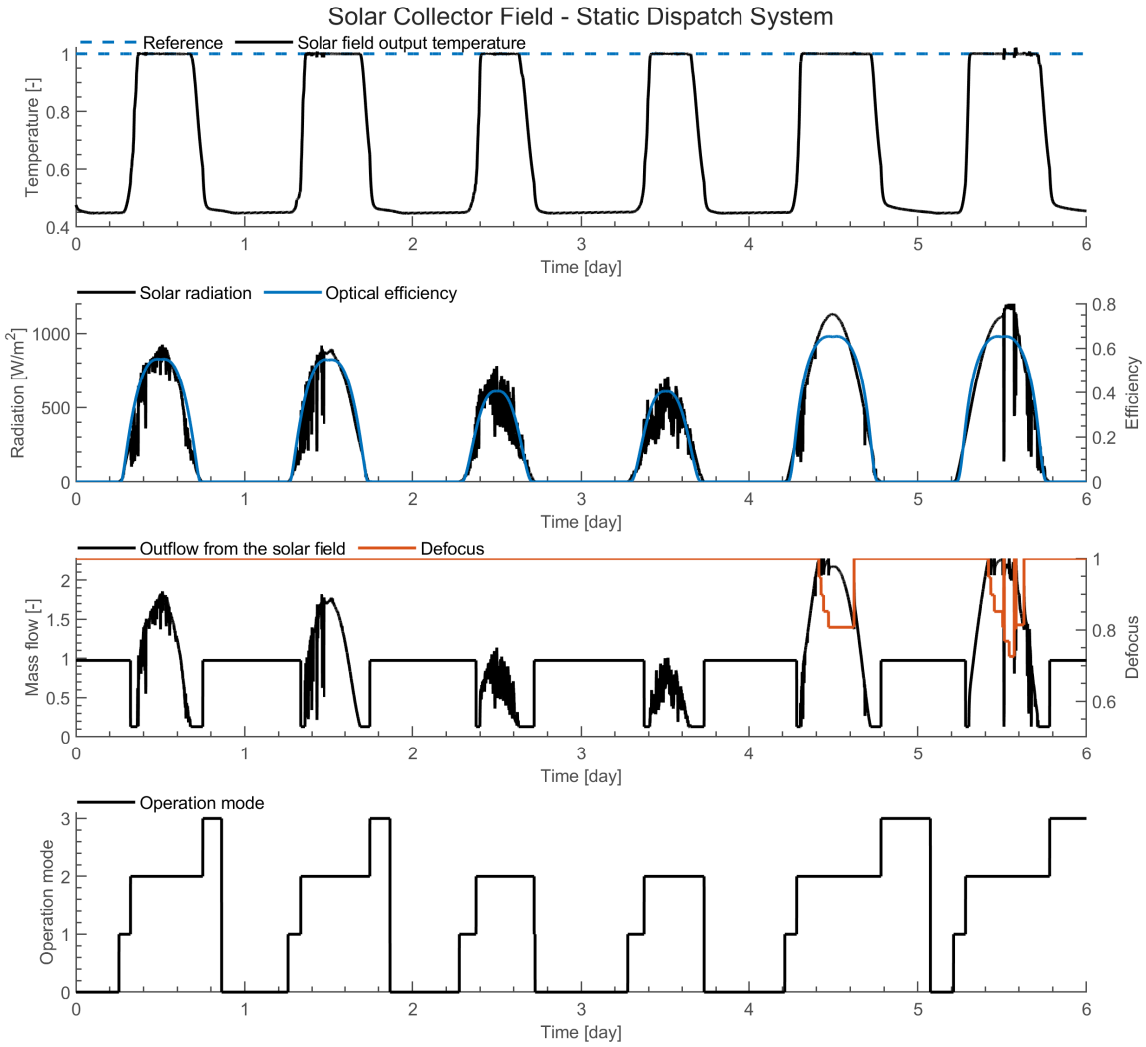

Figure 16 – Simulation results of the plant with the Classic Control Strategy and Static Dispatch System. From top to bottom, the graphics show: the outlet temperature of the field, solar irradiation and optical efficiency, defocus, mass flow rate in the solar field and operation modes.

The start-up operation mode is defined as the same maximum mass flow rate as, during the night. This approach proves to be faster to reach the value specified by recirculation temperature T_{rec}. During the normal operation mode, the reference tracking of the outlet temperature of the solar collector field is performed by a PI controller.

5.1.2.2 Thermal Energy Storage

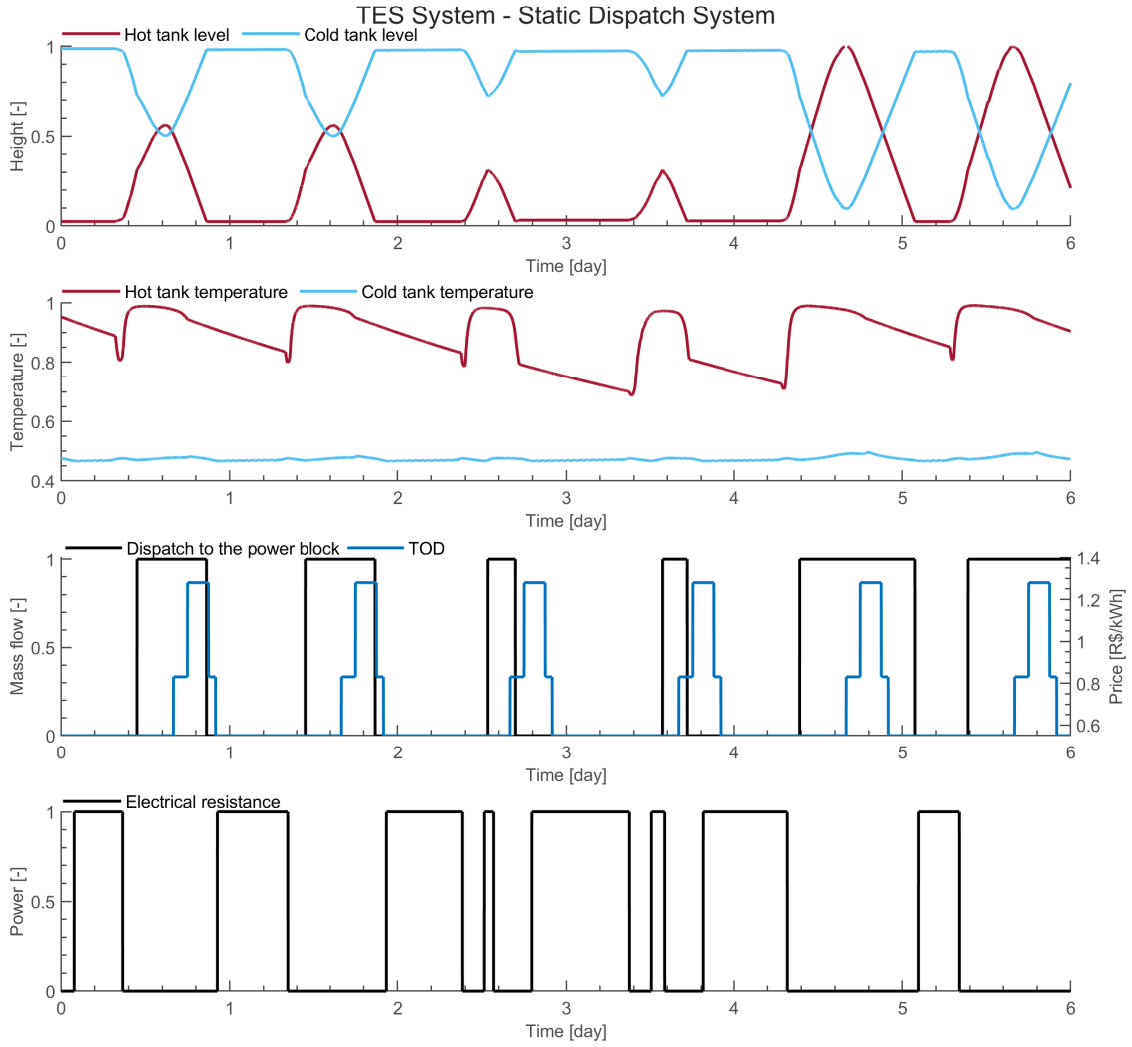

Figure 17 – Simulation results of the plant with the Classic Control Strategy and Static Dispatch System. From top to bottom, the graphics show: liquid levels in the storage tanks, HTF temperature in the storage tanks, dispatch mass flow and TOD, and electrical power induced by the resistance in the cold TES.

The biggest difference concerning optimal control is when analyzed the time evolution of the variables associated with the TES system, as presented in Figure 17. The dispatch is set to handle the worst-case scenario, which is the reason why this approach starts dispatching early in some days even with a low radiation profile (time

interval between days 1 and 4), on the other hand, it presents better results in days with high solar radiation (days 5 and 6, as can be seen in the third graphic of Figure 17). It is important to emphasize that the simulation of the solar collector field and the TES system are performed in parallel, i.e., the temperature of the cold TES is the inlet temperature of the solar collector field.

5.1.3 Classic Control Strategy - Dynamic Dispatch System

5.1.3.1 Solar Collector Field

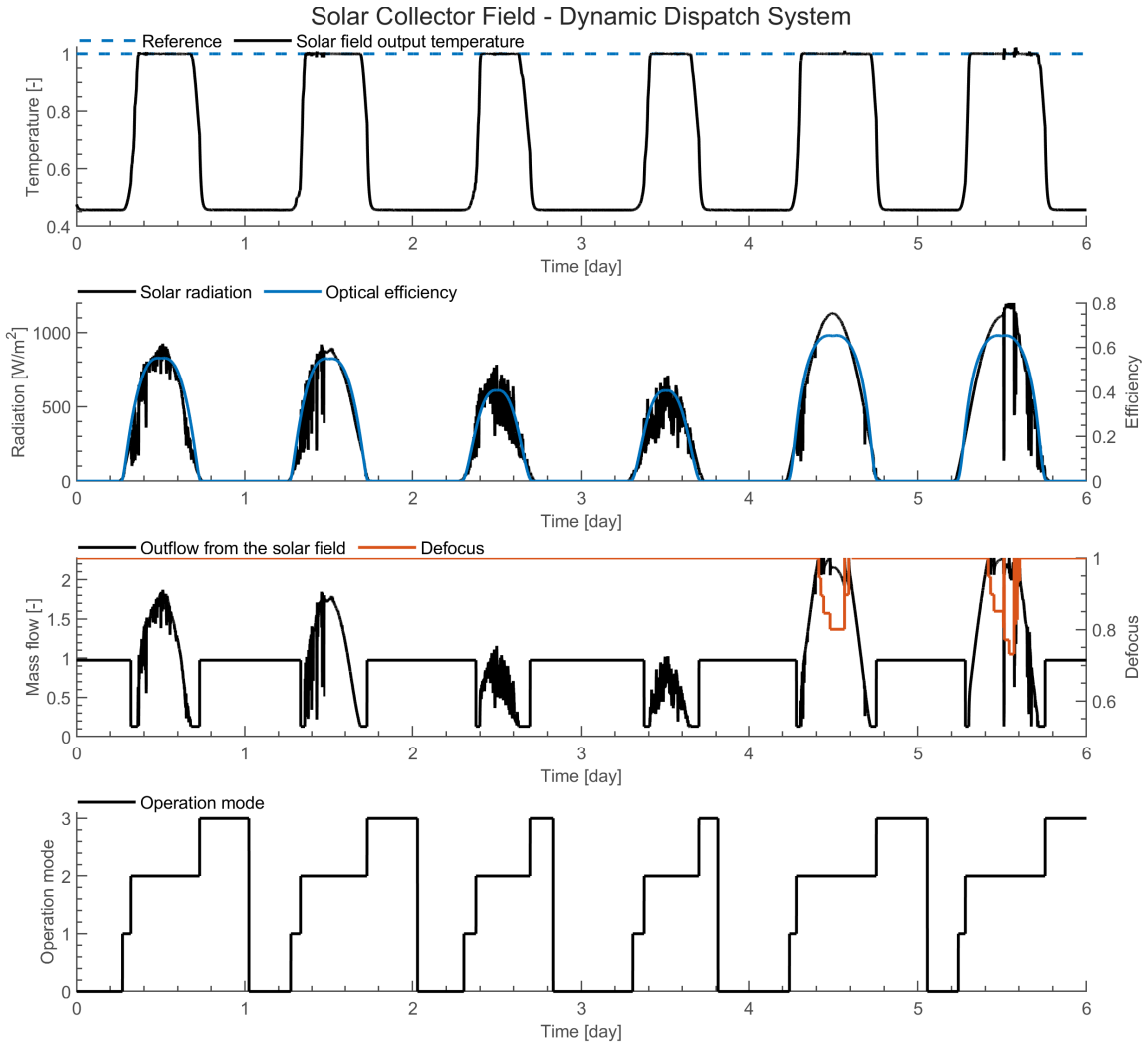

Figure 18 – Simulation results of the plant with the Classic Control Strategy and Dynamic Dispatch System. From top to bottom, the graphics show: the outlet temperature of the field, solar irradiation and optical efficiency, defocus, mass flow rate in the solar field and operation modes.

Figure 18 presents the time evolution of the main variables of the solar collector field within the Classic Control Strategy using the Dynamic Dispatch System. As already described in Chapter 4, the solar field is simulated first, independently, assuming

that the entry temperature of the solar collector is constant. This approximation signs reasonable, whereas the temperature of the cold TES is maintained in a small operating range. It is possible to observe that the reference tracking, mass flow rate, and defocus are similar to the Classic Control with the Static Dispatch System.

5.1.3.2 Thermal Energy Storage

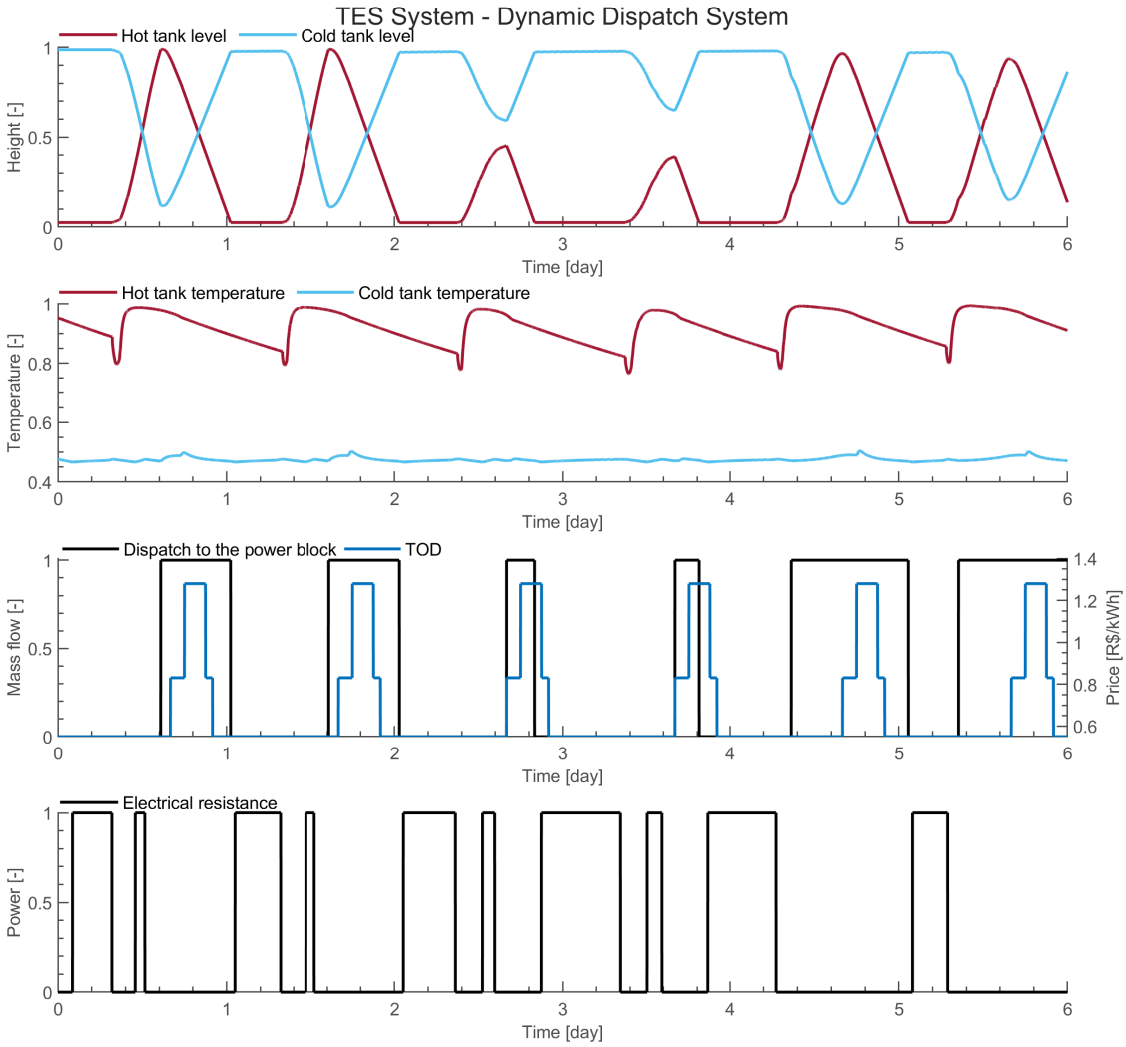

Figure 19 – Simulation results of the plant with the Classic Control Strategy and Dynamic Dispatch System. From top to bottom, the graphics show: liquid levels in the storage tanks, HTF temperature in the storage tanks, dispatch mass flow and TOD, and electrical power induced by the resistance in the cold TES.

In Figure 19 are presented time evolution of the variables associated with the TES system. It is important to highlight that the simulation of the TES system is now done independently considering the temperature and mass flow rate of the solar field performed before. The algorithm of the Dynamic Dispatch System can find the priority

dispatch list based on the temperatures and mass flow rates futures of the solar field. The controller provides a better handle of the storage system, as can be seen in the third graphic of Figure 19 in the time days 1, 2, 5, and 6 when the dispatch only occurs by saturation time dispatch. On days 3 and 4, with low solar radiation, the dispatch is updated to the priority price times. In this approach, the priority dispatch list is calculated day after day, allowing to presents an improvement in the results in the time to sell electricity compared to the previous controller. Also, it is possible to notice that the controller can avoid saturation on the TES system.

5.1.4 Discussions

In order to highlight the effectiveness of the proposed controller, a comparative study with the strategies described in Chapter 4 will be presented in this section. All the strategies were simulated for a period of 365 days considering the same TOD and electrical tariffs described in Section 5.1, and also radiation, ambient temperature, and optical efficiency data from the same geographic location of the Brazilian numerical scenario. For sake of brevity and space limitations, the graphics of the temporal evolution of the states will be omitted. The analysis will focus on the revenue of each strategy.

The heat map of the fluid dispatched to the power block for the Optimal Control, Static Dispatch System and Dynamic Dispatch System are shown in Figures 20, 21 and 22, respectively. The dark blue color refers to the null mass flow rate and the yellow color to the maximum mass flow rate. As already described in Chapter 4, the Classic Control Strategy with Static Dispatch System is tuned Static from the available solar irradiation data, and therefore, dispatch prediction errors are common on days of low solar radiation. Note that for months with abundant solar radiation, such as January and December, the adjustment of the dispatch of this strategy must be anticipated so that the hot TES does not saturate. In some cases, this causes the energy in the hot TES to be dispatched at times without the best electricity tariff prices. The Dynamic Dispatch System strategy presents better results over the Static Dispatch System strategy since dispatch is now dynamically calculated day by day, better handling with fluid storage and dispatch at priority times. However, in days with low solar radiation, the dispatch of the thermal transfer fluid to the power block ends up not being well distributed for periods of higher tariff. On the other hand, the proposed optimal strategy manages to anticipate the sale of electricity, without saturation of the storage tanks, while guaranteeing the maximum revenue.

The annual revenue gain of the optimal strategy in relation to the classic controller with Static Dispatch System for weather data of 2018 was 13.63% and for the Dynamic Dispatch System was 7.87%.

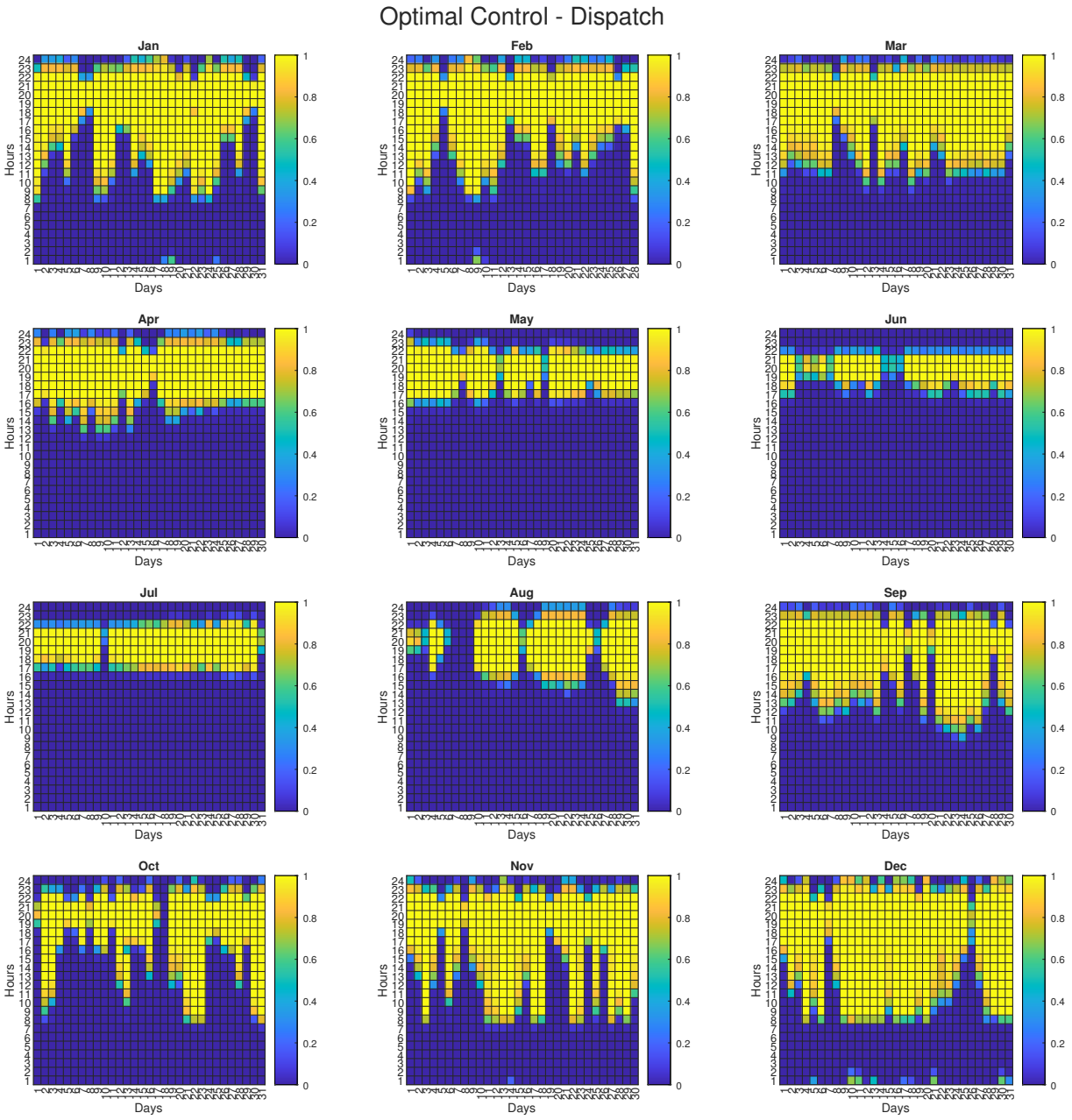

Figure 20 – Heat map of the fluid dispatch to the power block, Optimal Control (2018).

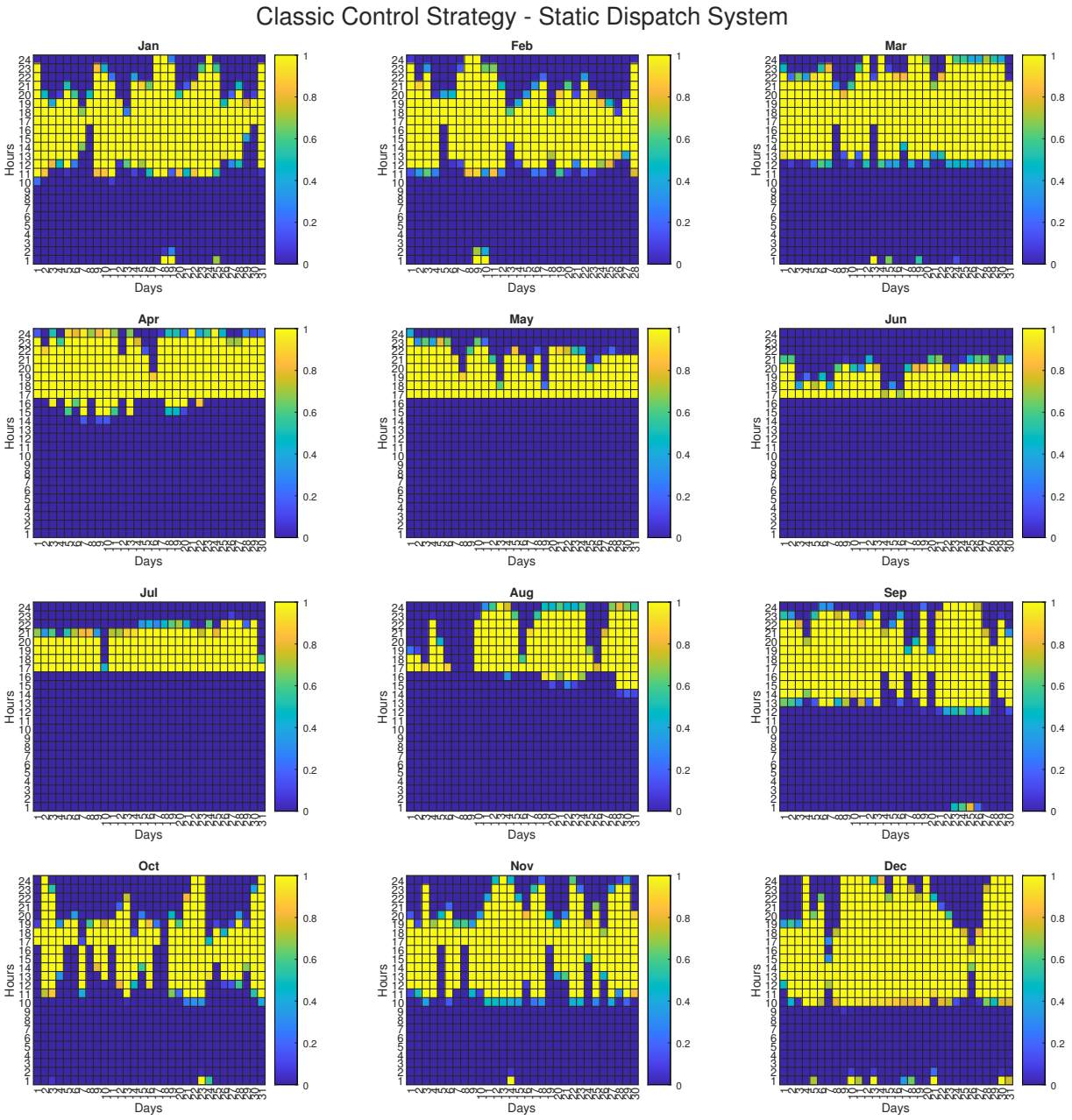

Figure 21 – Heat map of the fluid dispatch to the power block, Static Dispatch System (2018).

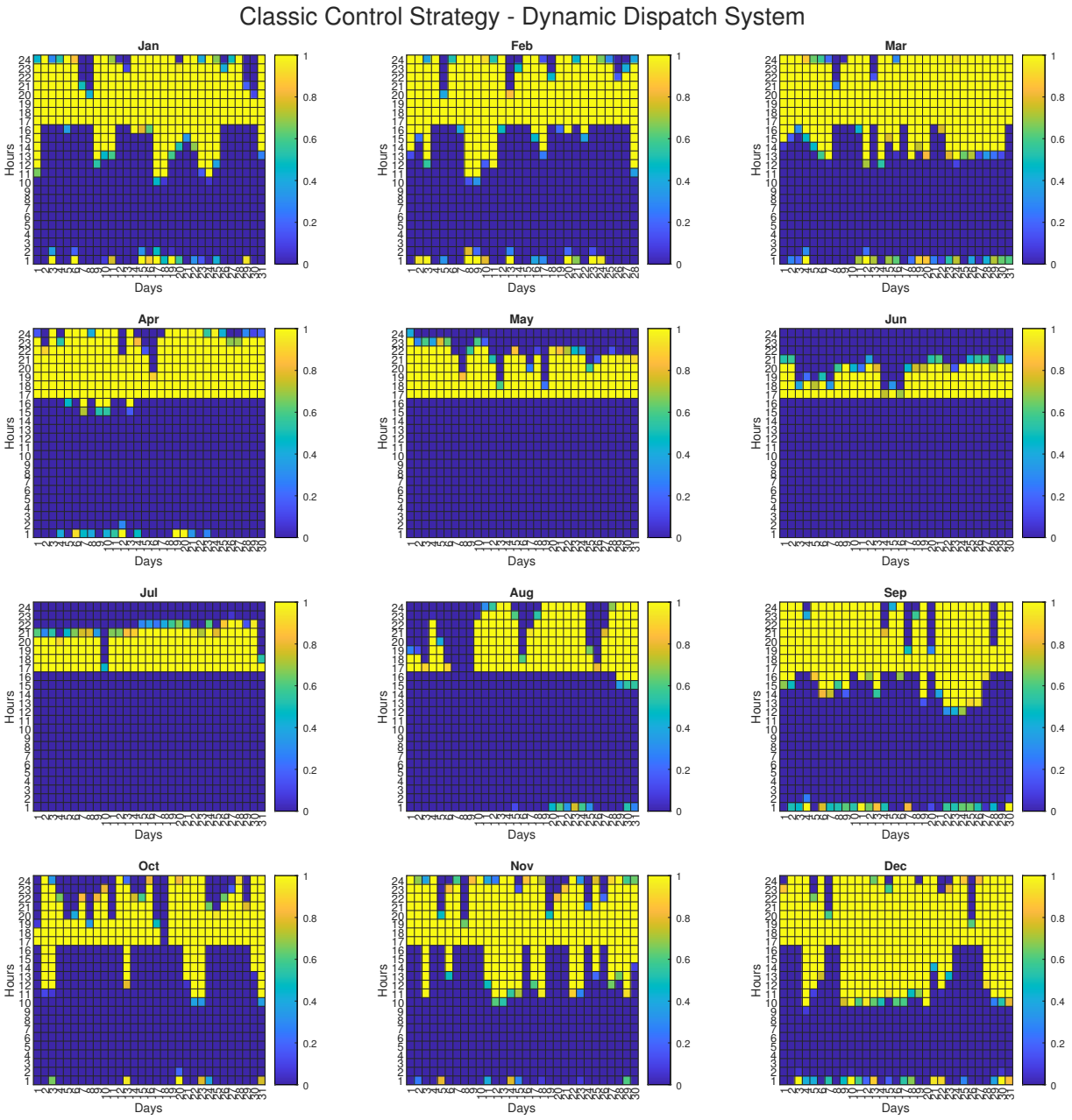

Figure 22 – Heat map of the fluid dispatch to the power block, Dynamic Dispatch System (2018).

5.2 SIMULATION RESULTS FOR THE SPANISH ENERGY TARIFF PRICE

The proposed optimal strategy was also tested for the Spanish energy tariff price. The choice of Spain as the location of study was based on the fact that renewable energy technologies represent a significant fraction of the total electricity generation in that country (IRENA, 2018). The real data of solar radiation and ambient temperature correspond to the geographic location 37º05'27.8"N 2º21'19.0"W. Although the same solar plant from the previous section was used for this numerical scenario, the minimum operating mass flow rate to the power block had to be changed to $m_p^{mop} = 0.72$ and the control parameters re-tuned to obtain satisfactory behavior for this case.

It is important to emphasize that only 6 days of solar irradiation and ambient temperature data were available for this scenario, in contrast to the Brazilian scenario described in the previous section, which had a 365-day data set.

The general operation of the economic and electricity markets of the country are coordinated by the Mercado Ibérico de Eletricidade (MIBEL), a cooperation process funded by the governments of Portugal and Spain. This market has been established in Europe since 2014 and was crucial to achieve the objective of the European Internal Energy Market. The development of this liberalized energy market brings advantages for participants, who can choose to purchase and sell energy using the bilateral contracting model, whose operation is based on the conclusion of a contract, and it is possible to freely negotiate prices, volumes, and clauses or through the stock market with specifically known and transparent prices. In the MIBEL, the day-ahead price in the stock market is the responsibility of the Iberian Energy Market Operator (OMIE) (Spanish Pole) and aims to handle electricity transactions for the following day through the submission of electricity sale and purchase bids by the market participants, as an integral part of the electric power production, more information is presented in OMIE (2021b). The day-ahead market hourly price in Spain for the year 2021 is available in OMIE (2021a) and is used to perform the simulations in the following subsections.

5.2.1 Optimal Control

5.2.1.1 Solar Collector Field

Figure 23 shows the time evolution of the main variables of the solar collector field with the Optimal Control Strategy for the Spanish energy tariff price. This numerical scenario considers the plant operating over six days[2] with radiation profiles of clean and cloudy days in order to impose a wide range of operating conditions and optical efficiency values (see the second graphic of Figure 23). As can be seen in the first graphic of Figure 23, the optimal controller was able to track the outlet temperature reference during the day. The defocus was necessary only in the first day.

[2] Three days with good radiation in June and three days with low radiation in January, the reason why the optical efficiency and radiation intensity changes during these days.

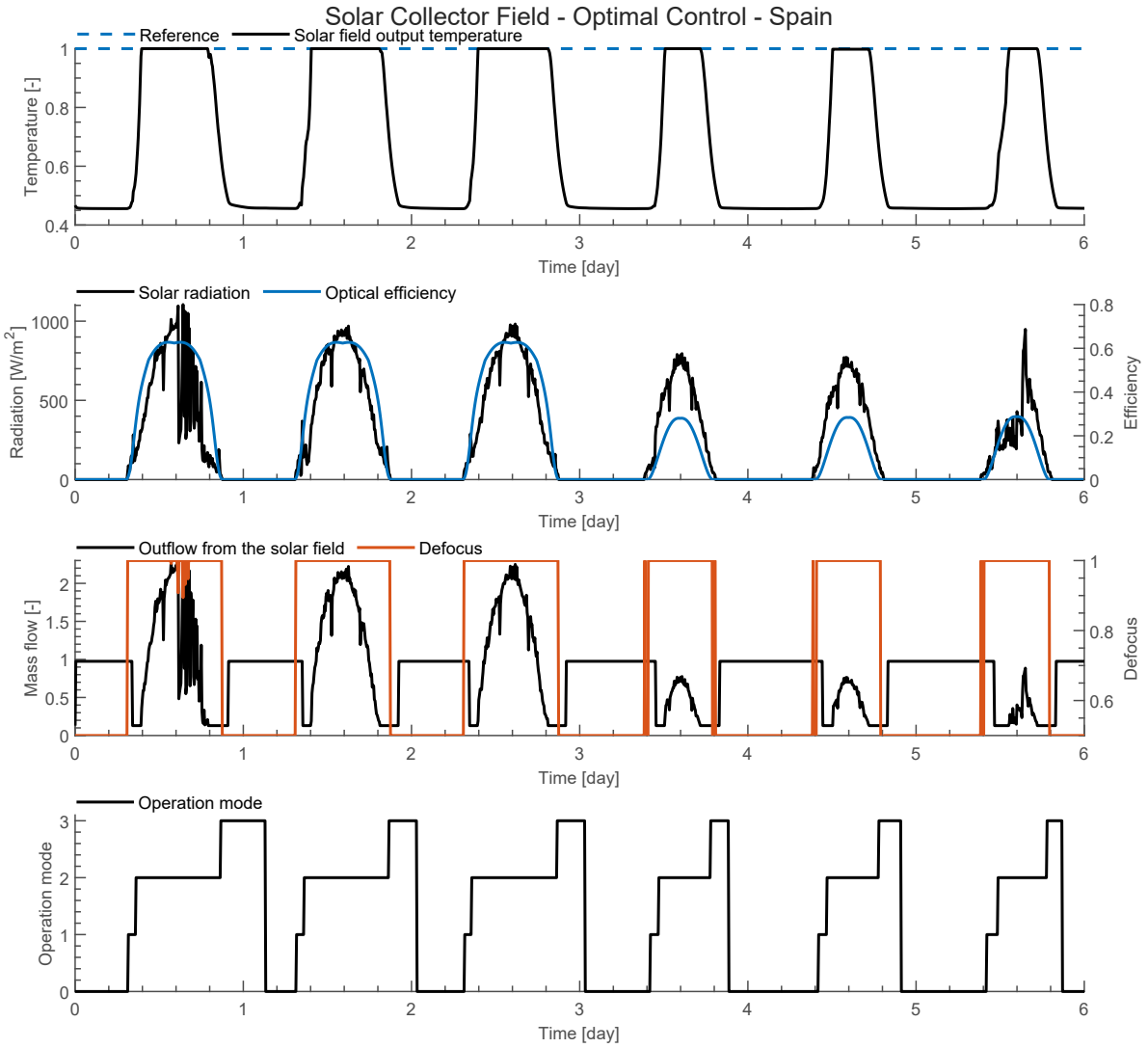

Figure 23 – Simulation results of the plant in the Spanish scenario with the Optimal Control Strategy. From top to bottom, the graphics show: the outlet temperature of the field, solar irradiation and optical efficiency, defocus, mass flow rate in the solar field and operation modes.

5.2.1.2 Thermal Energy Storage

The time evolution of the variables associated with the TES are presented in Figure 24. The level and temperature of the hot and cold TES are shown in the first and second graphics of Figure 24. The levels of both tanks stay within the designed operating range, without saturation. Electrical resistance for the first three days is almost only used during the night. However, for the days of low radiation profile, the electrical resistance remains active for almost the whole day to keep the temperature of the cold TES in the reference range.

The optimal controller always dispatches the fluid in the hot TES system to the power block during the time interval with better tariff prices. It is important to emphasize that the optimal control searches for the best time for dispatch day by day and always

dispatches all the fluid stored during the same day. Finally, note that the controller respects the new minimum operating mass flow rate limits to the power block, defined by m_p^{mop}, at the same time that it does not present repeated restarts during the same day when the dispatch starts.

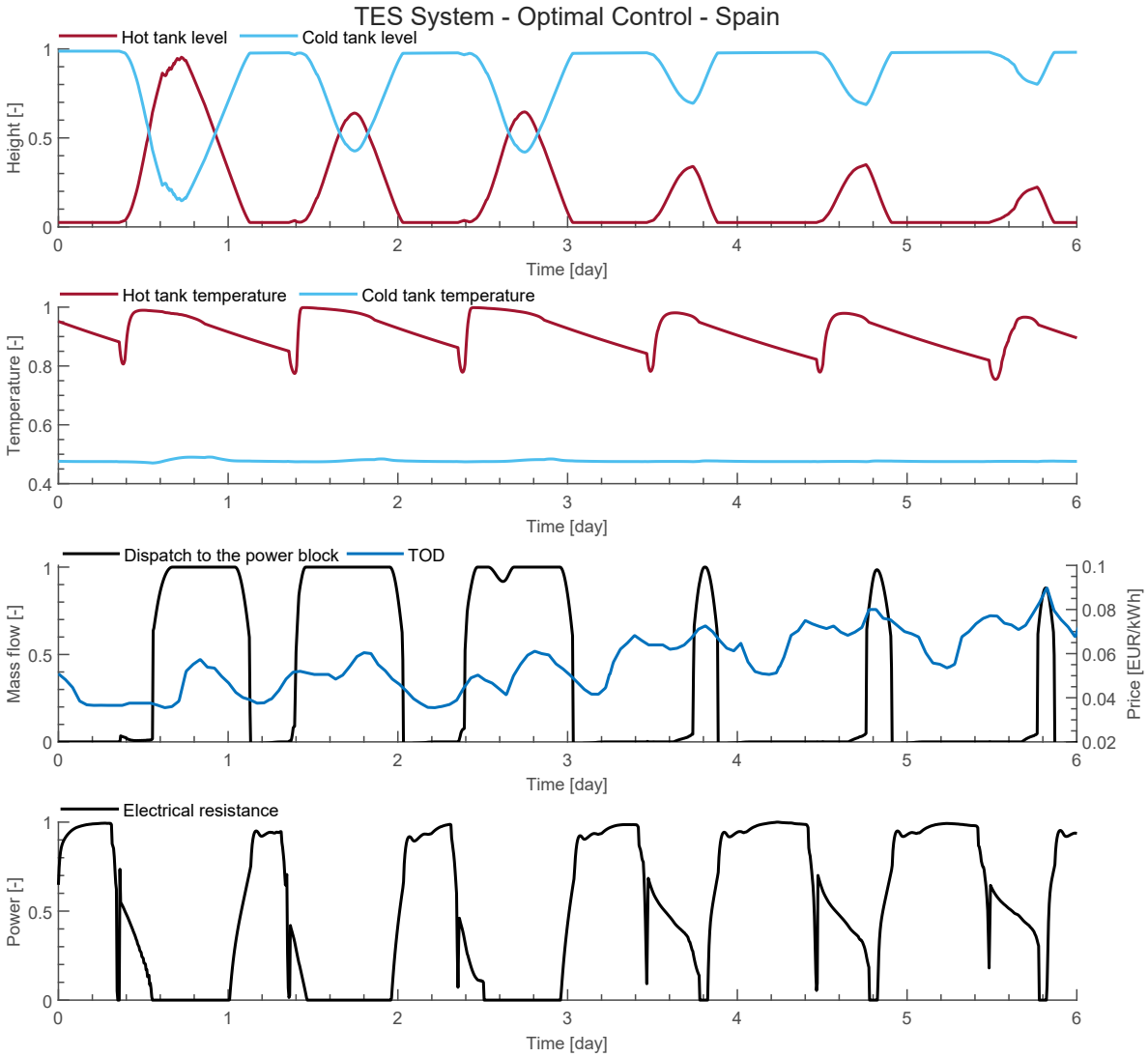

Figure 24 – Simulation results of the plant in the Spanish scenario with the Optimal Control Strategy. From top to bottom, the graphics show: liquid levels in the storage tanks, HTF temperature in the storage tanks, dispatch mass flow and TOD, and electrical power induced by the resistance in the cold TES.

5.2.2 Classic Control Strategy - Dynamic Dispatch System

5.2.2.1 Solar Collector Field

Figure 25 presents the time evolution of the main variables of the solar collector field within the Classic Control Strategy using the Dynamic Dispatch System for the Spanish energy tariff price. As already described in Chapter 4, the solar field is simulated first, independently, assuming that the entry temperature of the solar collector is

constant. This approximation signs reasonable, whereas the temperature of the cold TES is maintained in a small operating range. As can be seen in the first graphic of Figure 25, the controller was able to track the outlet temperature reference during the day. However, now the defocus is activated during the first three days.

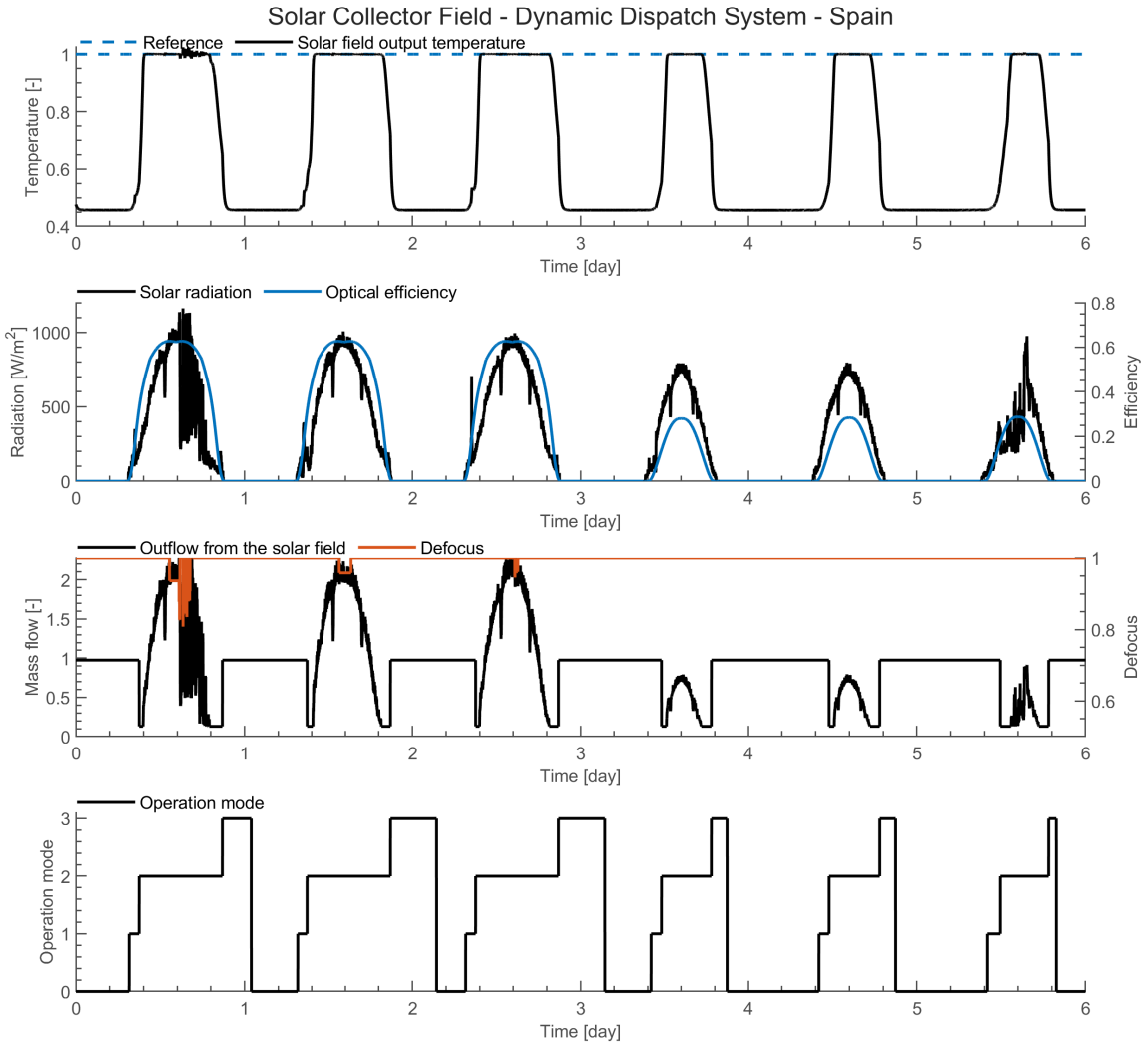

Figure 25 – Simulation results of the plant in the Spanish scenario with the Classic Control Strategy and Dynamic Dispatch System. From top to bottom, the graphics show: the outlet temperature of the field, solar irradiation and optical efficiency, defocus, mass flow rate in the solar field and operation modes.

5.2.2.2 Thermal Energy Storage

In Figure 26 are presented the time evolution of the variables associated with the TES system. It is important to highlight that the simulation of the TES system is now simulated independently considering the temperature and mass flow rate of the solar field performed before. The controller handles the storage system trying to dispatching the HTF in time intervals with better tariff prices, as can be seen in the third graphic of

Figure 26 in the time days 1, 2, and 3 when the dispatch only occurs by saturation time dispatch. On days 4, 5, and 6, with low solar radiation, the dispatch is updated to the priority price times. In this approach, defining priority price times to dispatch is difficult since the price varies during the day, on the other hand, the optimal controller always finds the better time to sell electricity.

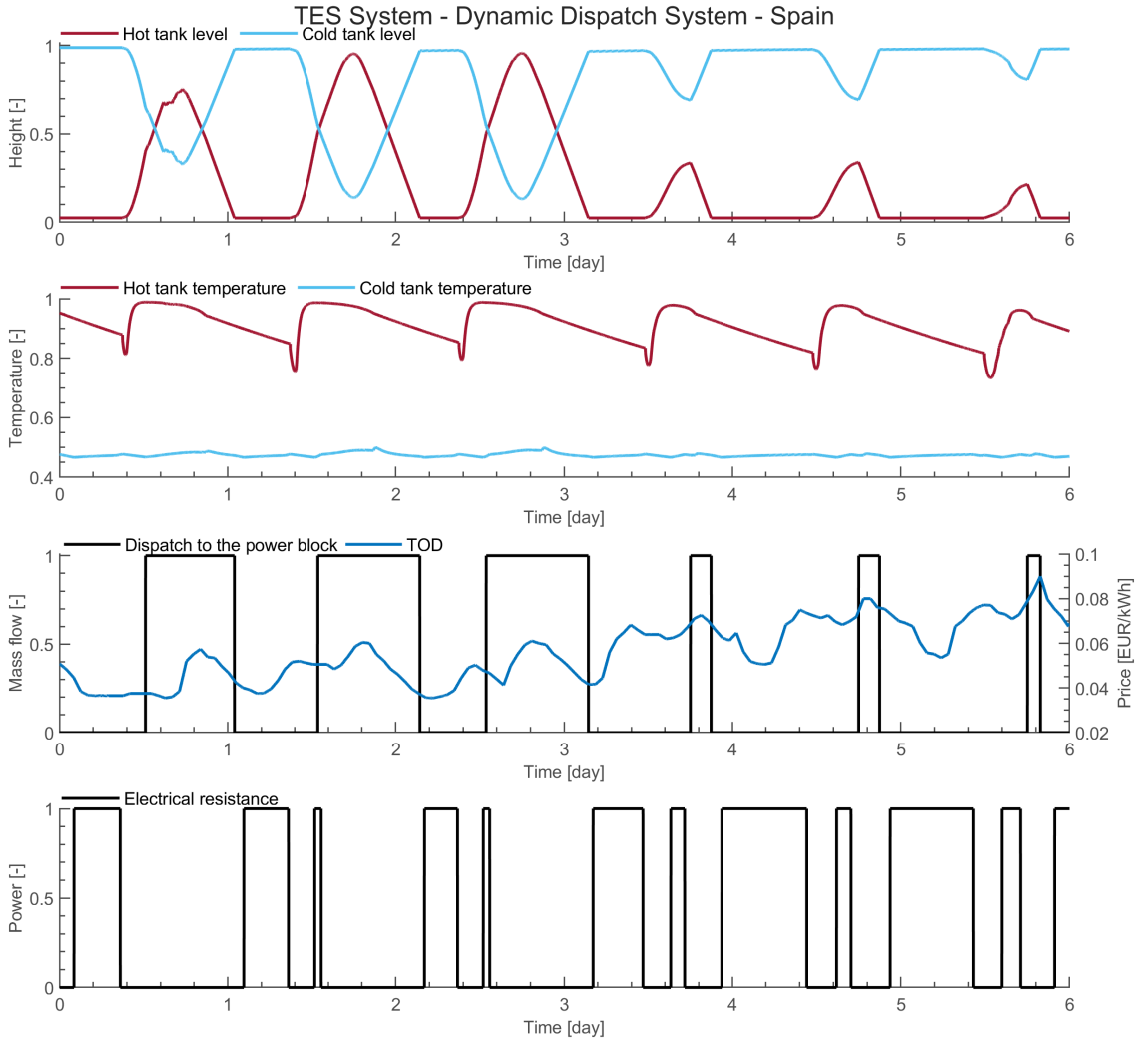

Figure 26 – Simulation results of the plant in the Spanish scenario with the Classic Control Strategy and Dynamic Dispatch System. From top to bottom, the graphics show: liquid levels in the storage tanks, HTF temperature in the storage tanks, dispatch mass flow and TOD, and electrical power induced by the resistance in the cold TES.

5.2.3 Discussions

The heat map of the fluid dispatches to the power block for the Classic Control Strategy with Dynamic Dispatch System and Optimal Control Strategy for the Spanish scenario are show in Figures 27 and 28, respectively. Both strategies were simulated for a period of 6 days considering the same TOD and electrical tariffs described in Section

5.2, and also radiation, ambient temperature, and optical efficiency data from the same geographic location of the Spanish numerical scenario.

The revenue gain of the optimal strategy in relation to the classic controller with Dynamic Dispatch System for weather data of the 6 days was 5.45%.

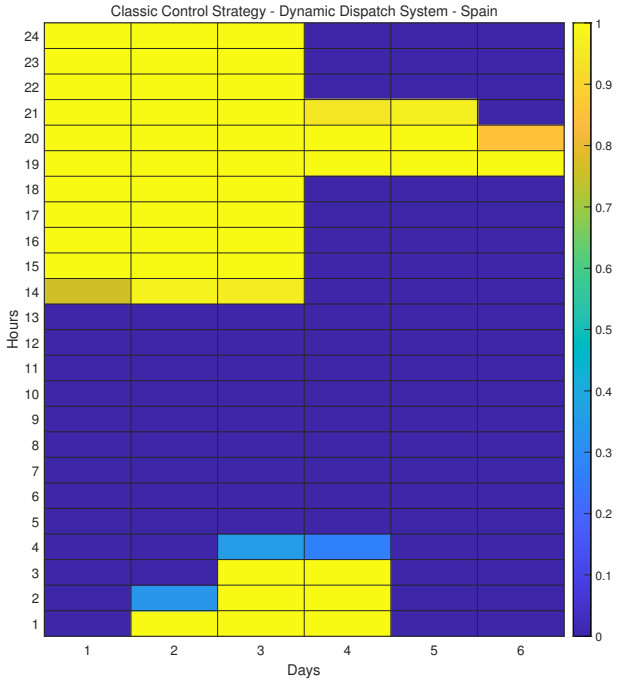

Figure 27 – Heat map of the fluid dispatch to the power block, Dynamic Dispatch System for the Spanish Energy Tariff Price.

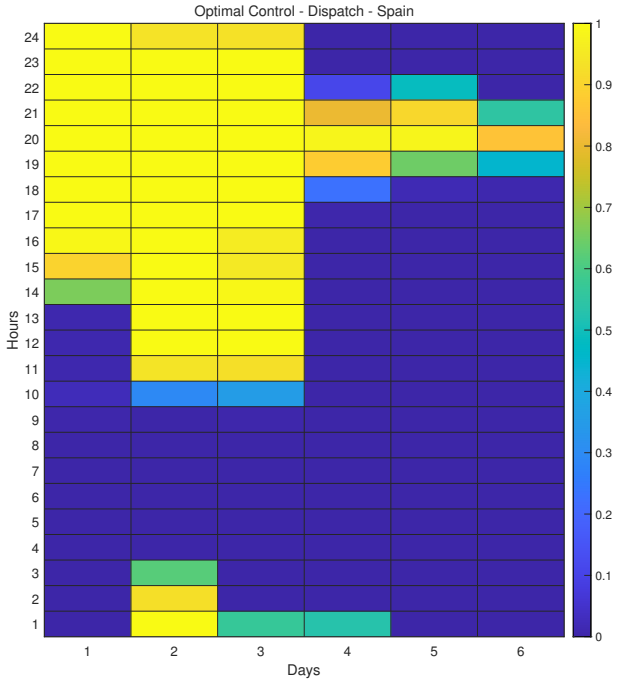

Figure 28 – Heat map of the fluid dispatch to the power block, Optimal Control for the Spanish Energy Tariff Price.

6 CONCLUSIONS

Solar thermal power plants are one of the most promising renewable energy options to substitute the increasing demand for conventional energy (REDDY et al., 2013). However, the cost per kW of solar power is still a disadvantage of these systems. Thus, much has been studied and developed in the literature to circumvent this problem and make solar thermal plants commercially viable.

This work focused on the study and application of an Optimal Control Strategy for solar thermal power plants with a thermal storage system in a variable energy tariff price. In such plants, the storage system and dispatch resources can be used to shift production to the most profitable hours, and consequently, the main control objective can be translated to maximize the solar energy captured in the solar collector field and the electrical energy revenue in the power block according to the energy tariff profile.

An important property of the configuration of the studied plant is the complete decoupling of the thermal process with the power block and the series coupling between the solar field and the TES system because it allows designing the control system in a decentralized manner: an optimal controller that aims to obtain the optimal trajectory of the solar collector field states by minimizing a cost function associated with the temperature reference tracking; and another one to compute the optimal control policy for the storage/dispatch of the TES system.

As a first step in the methodology, a simple mathematical model accounting for the main characteristics of the whole thermal process was proposed. Although the dynamic equations of the various subsystems involved are already well-established in the literature, it was necessary to perform a study and analysis on the coupling of the subsystems to ensure their correct operation. Then, the optimal controllers are designed considering these model equations plus the operational constraints.

The simulation results allowed to assess the potential of the proposal in order to increase the profitability of the plant in the Brazilian and Spanish energy tariff scenarios. Particularly, in one year of evaluation of the proposal with the Brazilian scenario, gains in revenue of up to 13.63% are obtained in relation to two classic control strategies. For plants operating in the context of time-varying tariffs, it is always profitable to exploit optimal controllers to the end of increasing the plant revenue. Notably, however, the system is only assessed for a specific condition of solar multiple and the results may vary depending on the conditions of storage capacity and size of the solar field.

It is important to emphasize that it was considered an ideal scenario of the control problem, that is, the knowledge of future solar radiation and the perfect combination of the model and the dynamics of the plant were considered. In this way, the attained performance represents a theoretical limit of the system operation, which in reality will have to face modeling errors, unmodeled disturbances, and uncertain weather forecasts.

This result may seem slightly optimistic but will represent the plant operation in a much more credible and perennial way than others obtained with simplified control policies.

6.1 CONTRIBUTIONS

Parts of this document were submitted in the following journal paper:

Paulo H. F. Biazetto, Gustavo A. de Andrade, and Julio E. Normey-Rico. Development of an optimal control strategy for temperature regulation and thermal storage operation of a solar power plant based on Fresnel collectors. IEEE Transactions on Control Systems Technology.

and in the following conference paper:

Paulo H. F. Biazetto, Gustavo A. de Andrade, and Julio E. Normey-Rico. Application of an optimal control strategy for solar power plants operating in a day-ahead market scheme. Simpósio Brasileiro de Automação Inteligente 2021.

6.2 FUTURE WORKS

Possible future works are listed bellow:

- To study and to analyze the robustness properties of the optimal control strategy. Due to the solar radiation forecasting and some variables and parameters estimation, the control policy can be degraded in a real-life application. In this case, it may be interesting to reformulate the controller in order to take into account the uncertainties in order to be able to produce experiments.
- To extend the proposed control methodology to other solar plant configurations such as those where the TES system operates in parallel with the solar collector field.
- To model and to design an optimal control strategy for the steam generation process.

REFERÊNCIAS

AGENCY, International Energy. **Key World Energy Statistics 2020**. [S.l.]: International Energy Agency, 2020a. P. 81. Available from: https://www.iea.org/reports/key-world-energy-statistics-2020.

AGENCY, International Energy. **World Energy Balances 2020**. [S.l.]: International Energy Agency, 2020b. (Statistics).

ALBERSMEYER, Jan; DIEHL, Moritz. The lifted Newton method and its application in optimization. **SIAM Journal on Optimization**, SIAM, v. 20, n. 3, p. 1655–1684, 2010.

ALMERÍA, Plataforma Solar de. **Plataforma Solar de Almería Facilities**. 2021. Available from: http://www.psa.es/en/facilities/index.php. Visited on: 29 May 2021.

ALVA, G.; LIN, Y.; FANG, G. An overview of thermal energy storage systems. **Energy**, Elsevier, v. 144, p. 341–378, 2018.

ANDERSSON, Joel A E; GILLIS, Joris; HORN, Greg; RAWLINGS, James B; DIEHL, Moritz. CasADi – A software framework for nonlinear optimization and optimal control. **Mathematical Programming Computation**, Springer, v. 11, n. 1, p. 1–36, 2019. DOI: 10.1007/s12532-018-0139-4.

ANDRADE, GA; PAGANO, DJ; ALVAREZ, José Domingo; BERENGUEL, Manuel. A practical NMPC with robustness of stability applied to distributed solar power plants. **Solar Energy**, Elsevier, v. 92, p. 106–122, 2013.

ANEEL. **Resolução homologatória n○ 2666, de 10 de março de 2020**. 2020. Available from: http://www2.aneel.gov.br/cedoc/reh20202666ti.pdf. Visited on: 15 Apr. 2021.

ÅSTRÖM, K. J.; HÄGGLUND, T. **Advanced PID control**. Research Triangle Park, USA: ISA - The Instrumentation, Systems, and Automation Society, 2005.

ATHANS, M.; FALB, P.L. **Optimal Control: An Introduction to the Theory and Its Applications**. [S.l.]: Dover Publications, 2007. (Dover Books on Engineering). ISBN 9780486453286.

BACHELIER, C.; STIEGLITZ, R. Design and optimisation of linear Fresnel power plants based on the direct molten salt concept. **Solar Energy**, v. 152, p. 171–192, 2017.

BARAO, M; LEMOS, JM; SILVA, RN. Reduced complexity adaptive nonlinear control of a distributed collector solar field. **Journal of process control**, Elsevier, v. 12, n. 1, p. 131–141, 2002.

BETTS, John T. **Practical methods for optimal control and estimation using nonlinear programming**. [S.l.]: SIAM, 2010.

BOCK, Hans Georg; EICH-SOELLNER, Edda; SCHLÖDER, Johannes P. **Numerical solution of constrained least squares boundary value problems in differential algebraic equations**. [S.l.]: Sonderforschungsbereich 123, 1987.

BOCK, Hans Georg; PLITT, Karl-Josef. A multiple shooting algorithm for direct solution of optimal control problems. **IFAC Proceedings Volumes**, Elsevier, v. 17, n. 2, p. 1603–1608, 1984.

BONVIN, D.; SRINIVASAN, B. On the role of the necessary conditions of optimality in structuring dynamic real-time optimization schemes. **Computers and Chemical Engineering**, v. 51, p. 172–180, 2013.

CAMACHO, E. F.; RUBIO, F. R.; BERENGUEL, M.; L., Valenzuela. A survey on control schemes for distributed solar collector fields. Part I: Modeling and basic control approaches. **Solar Energy**, v. 81, n. 10, p. 1240–1251, 2007a.

CAMACHO, E. F.; RUBIO, F. R.; BERENGUEL, M.; L., Valenzuela. A survey on control schemes for distributed solar collector fields. Part II: Advances control approaches. **Solar Energy**, v. 81, n. 10, p. 1252 1272, 2007b.

CAMACHO, E.F.; BERENGUEL, M.; RUBIO, F. R.; MARTÍNEZ, D. **Control of solar energy systems**. London: Springer-Verlag, 2012.

CASATI, Emiliano; CASELLA, Francesco; COLONNA, Piero. Design of CSP plants with optimally operated thermal storage. **Solar Energy**, Elsevier, v. 116, p. 371–387, 2015.

CIRRE, Cristina M; BERENGUEL, Manuel; VALENZUELA, Loreto; CAMACHO, Eduardo F. Feedback linearization control for a distributed solar collector field. **Control Engineering Practice**, Elsevier, v. 15, n. 12, p. 1533–1544, 2007.

CLARKE, F.; DE PINHO, M. **Optimal control problems with mixed constraints.** [S.l.]: SIAM Journal on Control and Optimization, 2010.

EGELAND, Olav; GRAVDAHL, Jan Tommy. **Modeling and simulation for automatic control**. [S.l.]: Marine Cybernetics Trondheim, Norway, 2002. v. 76.

GAMBKRELIDZE, R. V. Discovery of the maximum principle. **Journal of Dynamical and Control Systems**, v. 5, p. 437–457, 1999.

GONZÁLEZ-PORTILLO, Luis F; MUÑOZ-ANTÓN, Javier; MARTINEZ-VAL, José M. An analytical optimization of thermal energy storage for electricity cost reduction in solar thermal electric plants. **Applied Energy**, Elsevier, v. 185, p. 531–546, 2017.

HOWLETT, P. G.; PUDNEY, P. J.; VU, X. Local energy minimization in optimal train control. **Automatica**, Elsevier, v. 45, n. 11, p. 2692–2698, 2009.

INPE. **Sistema de Organização Nacional de Dados Ambientais**. 2019. Available from: http://sonda.ccst.inpe.br/basedados/florianopolis.html. Visited on: 1 Mar. 2019.

IRENA, EC. Renewable energy prospects for the European Union. **International Renewable Energy Agency (IRENA), European Commission (EC), Abu Dhabi**, 2018.

LEEK, Viktor. **An optimal control toolbox for MATLAB based on CasADi**. [S.l.: s.n.], 2016.

LEMOS, João M; NEVES-SILVA, Rui; IGREJA, José M. **Adaptive control of solar energy collector systems**. [S.l.]: Springer, 2014. v. 253.

LIBERZON, D. **Calculus of Variations and Optimal Control Theory: A Concise Introduction**. [S.l.]: Princeton University Press, 2012.

LIN, W. S.; ZHENG, C. H. Energy management of a fuel cell/ultracapacitor hybrid power system using an adaptive optimal-control method. **Journal of Power Sources**, v. 196, n. 6, p. 3280–3289, 2011.

LOPES, Telma; FASQUELLE, Thomas; SILVA, Hugo G; SCHMITZ, Kai. HPS2-Demonstration of molten-salt in parabolic trough plants-Simulation results from system advisor model. In: AIP PUBLISHING LLC, 1. AIP Conference Proceedings. [S.l.: s.n.], 2020. P. 110003.

MADAENI, Seyed Hossein; SIOSHANSI, Ramteen; DENHOLM, Paul. How thermal energy storage enhances the economic viability of concentrating solar power. **Proceedings of the IEEE**, IEEE, v. 100, n. 2, p. 335–347, 2011.

MAHMOUDIMEHR, J.; SEBGHATI, P. A novel multi-objective dynamic programming optimization method: Performance management of a solar thermal power plant as a case study. **Energy**, Elsevier, v. 168, p. 796–814, 2019.

MAHMOUDIMEHR, Javad; LOGHMANI, Leila. Optimal management of a solar power plant equipped with a thermal energy storage system by using dynamic programming method. **Proceedings of the Institution of Mechanical Engineers, Part A: Journal of Power and Energy**, SAGE Publications Sage UK: London, England, v. 230, n. 2, p. 219–233, 2016.

MEHOS, M.; PRICE, H.; CABLE, R.; KEARNEY, D.; KELLY, B.; KOLB, G.; MORSE, F. **Concentrating solar power best practices study**. [S.l.], 2020.

MINAS E ENERGIA, Ministério de. **Balanço Energético Nacional 2020: Ano base 2019**. [S.l.]: Empresa de Pesquisa Energética, Ministério de Minas e Energia, 2020a. P. 292.

MINAS E ENERGIA, Ministério de. **Plano decenal de expansão de energia 2030**. 2020b. Available from: https://www.epe.gov.br/sites-pt/publicacoes-dados-abertos/publicacoes/PublicacoesArquivos/publicacao-538/PDE%202030_EnvioMME_rv2.pdf. Visited on: 18 May 2021.

OMIE. **Day-ahead market hourly prices in Spain**. 2021a. Available from: https://www.omie.es/en/file-access-list. Visited on: 29 May 2021.

OMIE. **Day-ahead Market Operation**. 2021b. Available from: https://www.omie.es/sites/default/files/inline-files/day_ahead_market.pdf. Visited on: 29 May 2021.

PELAY, U.; LUO, L.; FAN, Y.; STITOU, D.; ROOD, M. Thermal energy storage systems for concentrated solar power plants. **Renewable and Sustainable Energy Reviews**, Elsevier, v. 79, p. 82–100, 2017.

QUIRYNEN, Rien. Numerical simulation methods for embedded optimization, 2017.

REDA, Ibrahim; ANDREAS, Afshin. Solar position algorithm for solar radiation applications. **Solar energy**, Elsevier, v. 76, n. 5, p. 577–589, 2004.

REDDY, V. S.; KAUSHIK, S. C.; RANJAN, K. R.; TYAGI, S. K. State-of-the-art of solar thermal power plants: A review. **Renewable and Sustainable Energy Reviews**, v. 27, p. 258–273, 2013.

SCIARRETTA, A.; BACK, M.; GUZZELLA, L. Optimal control of parallel hybrid electric vehicles. **IEEE Transactions on Control Systems Technology**, v. 12, n. 3, p. 352–363, 2004.

SIOSHANSI, Ramteen; DENHOLM, Paul. The value of concentrating solar power and thermal energy storage. **IEEE Transactions on Sustainable Energy**, IEEE, v. 1, n. 3, p. 173–183, 2010.

TIBA, C. **Atlas solamerico do Brasil**. [S.l.]: Editora Universitária da Universidade Federal do Pernambuco, 2000.

WAGNER, M.; GILMAN, P. **Technical manual for the SAM physical trough model**. [S.l.], 2011.

WITTMANN, Michael; ECK, Markus; PITZ-PAAL, Robert; MÜLLER-STEINHAGEN, Hans. Methodology for optimized operation strategies of solar thermal power plants with integrated heat storage. **Solar Energy**, Elsevier, v. 85, n. 4, p. 653–659, 2011.

WU, S.; DING, K.; CHENG, P.; SHI, L. Optimal scheduling of multiple sensors over lossy and bandwidth limited channels. **IEEE Transactions on Control of Network Systems**, v. 7, n. 3, p. 1188–1200, 2020.